Title
Cell-Autonomous Retinal Pigment Epithelium Dysfunction in Stargardt Disease

Author
Lenis, Tamara Lee

Publication Date
2017

Peer reviewed|Thesis/dissertation

UNIVERSITY OF CALIFORNIA

Los Angeles

Cell-Autonomous Retinal Pigment Epithelium Dysfunction in Stargardt Disease

A dissertation submitted in partial satisfaction of the requirements for the degree Doctor of Philosophy in Molecular, Cellular and Integrative Physiology

by

Tamara Lee Lenis

2017

ABSTRACT OF THE DISSERTATION

Cell-Autonomous Retinal Pigment Epithelium Dysfunction in Stargardt Disease

by

Tamara Lee Lenis

Doctor of Philosophy in Molecular, Cellular and Integrative Physiology

University of California, Los Angeles, 2017

Professor Gabriel H. Travis, Chair

Recessive Stargardt disease (STGD1) is a blinding juvenile macular degeneration caused by mutations in ATP-binding cassette subfamily A member 4 (ABCA4), a membrane protein thought to be exclusively expressed in photoreceptor outer segment (OS) discs. Its proposed function is an inward-directed flippase for *N*-retinylidene-phosphatidylethanolamine (*N*-ret-PE), the conjugate of retinaldehyde and phosphatidylethanolamine, across OS discs. In STGD1 patients and mice with a null mutation in ABCA4 (*Abca4*$^{-/-}$), excess free retinaldehyde irreversibly reacts with *N*-ret-PE to form toxic bisretinoids, which accumulate as lipofuscin pigments in the retinal pigment epithelium (RPE). Chapter 1 of this dissertation provides the first evidence that ABCA4 is expressed in human and murine RPE, with subcellular localization to endo-phagolysosomal membranes, thus suggesting that bisretinoids may be forming directly in the RPE, in addition to being secondarily deposited from phagocytosed OS. Chapter 2 reveals that transgenic mice expressing ABCA4 in the RPE, but not in the retina, had decreased autofluorescence and lipofuscin granules, greater photoreceptor preservation, and significant reduction of bisretinoid and complement factor C3b accumulation, confirming that RPE-specific

ABCA4 plays a functional role in RPE internal membranes, as it does in photoreceptor OS discs. Since bisretinoids in the RPE result in susceptibility to complement-mediated injury and failure to support the neurosensory retina, we attempted in Chapter 3 to rescue the phenotype in *Abca4*$^{-/-}$ mice by increasing expression of a major complement negative-regulatory protein (CRP), complement receptor 1-like protein y (CRRY), in the RPE. Subretinal injection of recombinant adeno-associated virus containing CRRY (AAV-CRRY) in *Abca4*$^{-/-}$ mice significantly increased RPE CRRY levels, while reducing the accumulation of C3b, total bisretinoids and RPE lipofuscin. Rescue of *Abca4*$^{-/-}$ mice using AAV-CRRY gene therapy suggests that modulation of the complement system by increasing expression of CRPs in the RPE may be a potential treatment strategy for retinopathies associated with complement dysregulation. Chapter 4 discusses the implications of this dissertation which 1) presents a previously undiscovered role for RPE-expressed ABCA4 to limit excess toxic bisretinoid formation directly in the RPE and thereby maintain RPE health, and 2) demonstrates that the pathophysiology of STGD1 involves cell-autonomous, bisretinoid-induced susceptibility to complement, which can be reduced by complement modulation in the RPE.

The dissertation of Tamara Lee Lenis is approved.

Dean Bok

Michael B. Gorin

Alapakkam Sampath

Hui Sun

Gabriel H. Travis, Committee Chair

University of California, Los Angeles

2017

Table of Contents

List of Figures

List of recurring abbreviations

11-*cis*-RAL	11-*cis*-retinaldehyde
A2E	*N*-retinylidene-*N*-retinyl-ethanolamine
A2PE	*N*-retinylidene-*N*-retinyl-phosphatidylethanolamine
A2PE-H_2	Dihydro-*N*-retinylidene-*N*-retinyl-phosphatidyl-ethanolamine
AAV	Adeno-associated virus
ABCA4	ATP-binding cassette subfamily A member 4
AF	Autofluorescence
AMD	Age-related macular degeneration
all-*trans*-RAL	All-*trans*-retinaldehyde
all-*trans*-RAL Dimer-PE	All-*trans*-retinaldehyde dimer phosphatidylethanolamine
BSA	Bovine serum albumin
C3	Complement component 3
C3b	C3 cleavage fragment with C3 convertase activity
C5	Complement component 5
CatD	Cathepsin D
CAV1	Caveolin 1
CD59	Cluster of differentiation 59
CFH	Complement factor H
CRALBP	Cellular retinaldehyde-binding protein
CRB1	Crumbs homolog 1
CRP	Complement regulatory protein
CRRY	Complement receptor 1-like protein y
DAF1	Complement decay accelerating factor, GPI anchored
DAF2	Complement decay accelerating factor, transmembrane isoform
DAPI	4',6-Diamidino-2-Phenylindole, Dihydrochloride
EM	Electron microscopy
ERG	Electroretinography
GAPDH	Glyceraldehyde-3-phosphate dehydrogenase
hfRPE	Human fetal RPE
HPLC	High performance liquid chromatography
ICC	Immunocytochemistry
IHC	Immunohistochemistry
iC3b	Inactivated C3b
Iso-A2E	Double bond isomer of A2E
LAMP1	Lysosome-associated membrane glycoprotein 1
LC3	Microtubule-associated protein 1 light chain 3B
MAC	Membrane attack complex
MCP/CD46	Membrane cofactor protein/Cluster of differentiation 46
MERTK	Mer proto-oncogene tyrosine kinase
Myc	c-Myc proto-oncogene protein
NGS	Normal goat serum
N-ret-PE	*N*-retinylidene-phosphatidylethanolamine
OCT	Optical cutting temperature
OS	Outer segment of photoreceptor
qRT-PCR	Quantitative real-time polymerase chain reaction

PE	Phosphatidylethanolamine
PBS	Phosphate buffered saline
RD8	Retinal degeneration 8
RDH10	Retinol dehydrogenase type-10
RDS	Retinal degeneration slow/Peripherin
RHO	Rhodopsin
RPE	Retinal pigment epithelium
RPE65	Retinoid isomerohydrolase (RPE-specific 65 kDa protein)
S.D.	Standard deviation
SOD-1, SOD-2	Superoxide dismutase 1, Superoxide dismutase 2
STGD1	Recessive Stargardt disease
ZO-1	Zonula occuldens protein 1

Acknowledgements

I would like to thank Dr. Roxana Radu and Dr. Gabriel Travis for their guidance and mentorship during my research program in their laboratories. I would also like to thank my thesis committee members, Dr. Alapakkam Sampath, Dr. Dean Bok, Dr. Michael Gorin, and Dr. Hui Sun, for their time and dedication. I am very appreciative of the financial support I received during my doctoral studies at UCLA. I would especially like to acknowledge my training program, the Specialty Training and Advanced Research program in ophthalmology (EyeSTAR) at the Stein Eye Institute/Department of Ophthalmology at UCLA. I would like to thank my EyeSTAR program coordinator, Dr. Joseph Demer for the opportunity and continued support. My research would not have been possible without assistance and collaboration from my colleagues in the laboratory and clinic. I would also like to acknowledge the current and former chairs of Molecular and Cellular Integrative Physiology graduate program at UCLA, Dr. James Tidball and Dr. Mark Frye, as well as the program coordinator, Yesenia Rayos. Finally, I would like to extend a special thank you to my parents John and Ariel, my husband Andrew, and my sons Theo and Ari, for their love, support and inspiration.

Chapters 1 and 2 of this thesis are in preparation for publication. Chapter 3 of this thesis is a version of the following publication: Lenis TL, Sarfare S, Jiang Z, Lloyd MB, Bok D, Radu RA. Complement Modulation in the Retinal Pigment Epithelium Rescues Photoreceptor Degeneration in a Mouse Model of Stargardt Disease. *Proceedings of the National Academy of Sciences*. 2017 Apr 11;114(15):3987-3992. PMID: 28348233. T.L.L., S.S., and R.A.R. designed research; T.L.L., S.S., Z.J., M.B.L., and R.A.R. performed research; T.L.L., S.S., M.B.L., D.B., and R.A.R. analyzed data; and T.L.L., S.S., and R.A.R. wrote the paper.

Biographical Sketch

NAME: Lenis, Tamara Lee

POSITION TITLE: Postdoctoral Scholar, Stein Eye Institute, Department of Ophthalmology, David Geffen School of Medicine at UCLA

EDUCATION/TRAINING:

INSTITUTION AND LOCATION	DEGREE	Completion Date	FIELD OF STUDY
Columbia University, New York, NY	B.A.	05/2007	Biology and Art History
Case Western Reserve University, Cleveland, OH	M.D., M.S.	05/2013	Medicine, Clinical Research
University of California Los Angeles – Olive View Medical Center, Sylmar, CA	PGY1-Internship	06/2014	Internal Medicine
University of California Los Angeles – Stein Eye Institute, Los Angeles, CA	Ph.D.	06/2017 (expected)	Molecular, Cellular, and Integrative Physiology
University of California Los Angeles – Stein Eye Institute, Los Angeles, CA	PGY2-4 Residency	06/2020 (expected)	Ophthalmology - EyeSTAR Program

PUBLICATIONS:

Lenis TL, Sarfare S, Jiang Z, Lloyd MB, Bok D, Radu RA. Complement Modulation in the Retinal Pigment Epithelium Rescues Photoreceptor Degeneration in a Mouse Model of Stargardt Disease. *Proceedings of the National Academy of Sciences*. 2017 Apr 11;114(15):3987-3992. PMID: 28348233.

Grossniklaus HE, **Lenis TL,** Jakobiec FA. Retinal Reactive Astrocytic Tumor (Focal Nodular Gliosis): The Entity Also Known as Vasoproliferative Tumor. *Ocular Oncology and Pathology.* 2017;3:161-163. https://doi.org/10.1159/000455149.

Lenis TL, Chiu SY, Law SK, Yu F, Aldave AJ. Safety of Concurrent Boston Type I Keratoprosthesis and Glaucoma Drainage Device Implantation. *Ophthalmology.* 2017 Jan;124(1):12-19. PMID: 27614591.

Lenis TL, Klufas MA, Randhawa S, Sharma M, Sarraf D. Posterior Polar Annular Choroidal Dystrophy: A Case Series. *Retinal Cases and Brief Reports.* 2017 Winter;11 Suppl 1:S24-S27. PMID: 27571427.

Ahmad S, Mathews PM, Srikumaran D, Aldave AJ, **Lenis TL,** Aquavella JV, Hannush SB, Belin M, Akpek EK. Outcomes of Repeat Boston Type 1 Keratoprosthesis Implantation. *American Journal of Ophthalmology*. 2016 Jan;161:181-7. PMID: 26482467.

Kuehlewein L, Dansingani KK, de Carlo TE, Bonini Filho MA, Iafe NA, **Lenis TL,** Freund KB, Waheed NK, Duker JS, Sadda SR, Sarraf D. Optical coherence tomography angiography of Type 3 Neovascularization secondary to Age-Related Macular Degeneration. *Retina*. 2015 Nov;35(11):2229-35. PMID: 26502007.

Kuehlewein L, Bansal M, **Lenis TL,** Iafe NA, Sadda SR, Bonini Filho MA, De Carlo TE, Waheed NK, Duker JS, Sarraf D. Optical Coherence Tomography Angiography of Type 1 Neovascularization in Age-Related Macular Degeneration. *American Journal of Ophthalmology.* 2015 Oct;160(4):739-48. PMID: 26164826.

Singh RP, **Lee TJ,** Yau L, Rubio R. Collateral vessel presence in branch and central retinal vein occlusions and their impact on visual acuity and anatomical gains: A retrospective analysis. *Retina.* 2014 Nov; 34(11):2242-9. PMID: 25046394.

Lee TJ, Hwang JC, Chen RW, Lima LH, Wang NK, Tosi J, Freund KB, Yannuzzi LA, Tsang SH. The Role of Fundus Autofluorescence in Late-Onset Retinitis Pigmentosa (LORP) Diagnosis. *Ophthalmic Genetics.* 2014 Sep; 35(3):170-9. PMID: 23899229.

Hoppe G, **Lee TJ*,** Yoon S, Yu M, Peachey NS, Rayborn M, Zutel MJ, Trichonas G, Au J, Sears JE. Inducing a visceral organ to protect a peripheral capillary bed: stabilizing hepatic HIF-1α prevents oxygen-induced retinopathy. *American Journal of Pathology*. 2014 Jun; 184(6):1890-9. PMID: 24731446. *Co-first authorship.

Lenis TL, Dhrami-Gavazi E, Lee W, Mukkamala SK, Tabacaru MR, Yannuzzi L, Gouras P, Tsang SH. Novel Compound Heterozygous Mutations Resulting in Cone Dystrophy With Supernormal Rod Response. *JAMA Ophthalmology*. 2013 Nov; 131(11):1482-5. PMID: 24029832.

Trichonas G, **Lee TJ,** Hoppe G, Au J, Sears JE. Prolyl hydroxylase inhibition during hyperoxia prevents oxygen-induced retinopathy in the rat 50/10 model. *Investigative Ophthalmology and Visual Science.* 2013 July; 54(7):4919-26. PMID 23761085.

Orge FH, **Lee TJ,** Walsh M, Gordon K. Comparison of fentanyl and morphine in laser surgery for ROP. *Journal of the American Association for Pediatric Ophthalmology and Strabismus.* 2013 Apr; 17(2):135-9. PMID 23622445.

Lee TJ, Kohn M, Young JB. Discovering full potential in academic medicine: a science and an art. *Academic Medicine*. 2012; 87(11): 1477. PMID 23111266.

Tan CC, Sindhu KV, Li S, Nishio H, Stoller JZ, Oishi K, Puttreddy S, **Lee TJ,** Epstein JA, Walsh MJ, Gelb BD. Transcription factor Ap2delta associates with Ash2l and ALR, a trithorax family histone methyltransferase, to activate Hoxc8 transcription. *Proceedings of the National Academy of Sciences*. 2008 May 27; 105(21): 7472-7477. PMID: 18495928.

Chapter 1: ABCA4 is expressed in the Retinal Pigment Epithelium (RPE)

i. Introduction

Physiologic function of ABCA4 in photoreceptor outer segments

The rod and cone photoreceptor cells in the vertebrate retina are responsible for initiating vision. They contain a structure called the outer segment (OS), comprising a stack of flattened membranous disks packed with rhodopsin or cone-opsin pigments. The photoisomerization of vitamin A-derived visual chromophore 11-*cis*-retinaldehyde (11-*cis*-RAL) to its all-*trans*-retinaldehyde (all-*trans*-RAL) isomer is the first and central step in visual signaling, and renewal of the visual pigment, which consists of a protein component (opsin) covalently bound to the photosensitive chromophore 11-*cis*-RAL, is required for vision[1]. Continuous vision is achieved by the recycling of all-*trans*-RAL back to 11-*cis*-RAL, through a series of enzymatic reactions involving reduction, acylation, isomerization and oxidation[2].

The ATP-binding cassette subfamily A, member 4 (ABCA4) transporter is a membrane protein involved in the visual cycle and it has been shown to be expressed in retinal photoreceptor outer segment (OS) discs[3-8]. Whereas most eukaryotic ABC transporters are exporters, outwardly translocating substrates from cytoplasmic to extracellular or luminal compartments, ABCA4 expressed in rod and cone OS discs is proposed to be an importer for *N*-retinylidene-phosphatidylethanolamine (*N*-ret-PE), the Schiff base adduct of retinaldehyde and PE[7,9-11]. By flipping *N*-ret-PE inwardly across OS disc membranes, photoreceptor-expressed ABCA4 is believed to facilitate the removal of all-*trans*-retinaldehyde (all-*trans*-RAL) via its subsequent reduction to all-*trans*-retinol by retinol dehydrogenase type-10 (RDH10) in the OS cytoplasm[11-14].

Thus, ABCA4 contributes to (i) visual pigment recycling for continuous photosensitivity and (ii) preventing build-up of reactive free all-*trans*-RAL which may form toxic bisretinoid adducts if present in excess. Mutations in ABCA4 cause recessive Stargardt disease (STGD1), which is the most common juvenile macular dystrophy with an estimated prevalence of 1 in 8,000-10,000 individuals[15-17].

ABCA4 expression in mammalian tissues

It is well established that ABCA4 is primarily expressed in retinal photoreceptor outer OS discs, however several studies have also suggested that ABCA4 mRNA and protein may be expressed in the choroid plexus of the brain and in skin fibroblasts[18,19]. Furthermore, systems-level analyses looking at genes expressed in developing RPE and in human fetal RPE cell culture have also identified *Abca4* gene expression in the RPE[20,21]. However, there have been no published studies to critically assess whether ABCA4 protein is present in the RPE (RPE-ABCA4).

The RPE and photoreceptors are interdependent adjacent cell layers of the outer retina that are required for visual function.[22] Isolation of the RPE-choroid-sclera eyecup from the rest of the neurosensory retina (herein referred to as “RPE” vs. “retina,” respectively) may result in inadvertent contamination with retina-specific protein during the dissection procedure. An additional source of retinal byproducts in the RPE comes from the daily phagocytic uptake and removal of the distal 10% of photoreceptor OS tips by the adjacent RPE.[23,24] Thus, the presence of retinal proteins in the RPE may possibly be attributed to this physiologic renewal process, which follows a circadian pattern mirroring cyclic light and sees its peak at approximately two hours following the onset of light.[25] A detailed analysis of RPE-specific expression should therefore avoid the phagocytic peak after light onset by timing tissue collections several hours after the time of light onset. Another strategy used in this work was to conduct RPE-specific

expression studies in wild type and *Abca4*$^{-/-}$ mice, in addition to mice with a null mutation in Mer proto-oncogene tyrosine kinase (*Mertk*$^{-/-}$) which result in loss of phagocytosis and near complete photoreceptor degeneration by two to three months of age.[26] By five months of age, *Mertk*$^{-/-}$ mice have one or two photoreceptor nuclei visible in the outer nuclear layer with no visible photoreceptor OS adjacent to the remaining RPE.

We conducted an extensive analysis to determine if ABCA4 is endogenously expressed in the RPE, given the potential clinical importance of RPE-expressed ABCA4 in the context of retinal physiology and disease. The presence of ABCA4 in the RPE alters our understanding of STGD1 pathophysiology by suggesting that it involves a cell-autonomous process, and thereby potentially expands treatment options. Chapter 1 of this study is the first work to show *endogenous* ABCA4 protein expression in the RPE, apart from its deposition secondary to daily OS phagocytosis by the RPE.

ii. Expression of ABCA4 in murine, bovine, and human RPE

ABCA4 is expressed in RPE cells

We employed several approaches to test whether ABCA4 is expressed in RPE cells. First we looked for evidence that the *ABCA4* mRNA is expressed in RPE cells. RNA-Seq analysis of bovine RPE showed presence of the *ABCA4* mRNA, with greatly reduced or absent expression of mRNAs for the photoreceptor-specific proteins: rhodopsin, melanopsin, cone m-opsin and cone s-opsin (Fig. 1.1A). RNA-Seq analysis of confluent hfRPE cells also showed expression of the *ABCA4* mRNA and other RPE mRNAs including those for Rpe65, bestrophin-1, and LRAT, with absent expression of mRNAs for the photoreceptor proteins, rhodopsin, melanopsin, cone m-opsin and cone s-opsin (Fig. 1.1A). We also quantitated levels of the *ABCA4* and *rhodopsin* mRNAs in confluent hfRPE cells and human retina from an adult

cadaveric donor by qRT-PCR normalizing to 18S rRNA. The *ABCA4* mRNA was present in both adult retina and hfRPE cells, while the *rhodopsin* mRNA was only present in retina (Fig. 1.1B). These data show that the mRNA for *Abca4* is endogenously expressed in RPE cells.

ABCA4 and RDS/peripherin are integral membrane proteins located in the rims of rod and cone OS disks[3-5,8]. To determine whether the ABCA4 protein is present in RPE cells, we performed immunoblot analysis on retina and RPE homogenates from five-month-old wild type (129/Sv) and *Mertk*$^{-/-}$ mice using antibodies against ABCA4 and RDS/peripherin (Fig. 1.2A). Both ABCA4 and RDS/peripherin were present in five-month-old wild type retina homogenates, but undetectable in *Mertk*$^{-/-}$ retinas of the same age (Figs. 1.2B and 1.2C), consistent with complete degeneration of photoreceptors in these animals[26]. Importantly, ABCA4 was present at ~20% of the wild type level in *Mertk*$^{-/-}$ RPE homogenates, while RDS/peripherin was virtually undetectable in the same samples. The persistence of ABCA4 immunoreactivity in RPE homogenates from fully degenerate *Mertk*$^{-/-}$ mice suggests that ABCA4 is endogenously expressed in RPE.

We also tested for ABCA4 expression in RPE cells by immunofluorescence analysis. Wild type (129/Sv) retinas showed ABCA4 immunofluorescence in photoreceptor OS and RPE cells, while degenerate *Mertk*$^{-/-}$ sections showed ABCA4 immunofluorescence only in the RPE (Fig. 1.3A). As expected, we observed no ABCA4 immunofluorescence in *Abca4*$^{-/-}$ retina/RPE sections (Fig. 3A). Primary cultures of human fetal RPE (hfRPE) cells were established before photoreceptor differentiation[27]. Immunofluorescence analysis on sections of hfRPE cells grown to confluence showed a granular pattern of ABCA4 immunoreactivity, consistent with a distribution in internal membranes (Fig. 1.3B). The presence of ABCA4 immunoreactivity in *Mertk*$^{-/-}$ RPE cells, which are incapable of OS phagocytosis, and in hfRPE cells, which were never exposed to photoreceptor OS, is further evidence that ABCA4 is endogenously expressed in RPE cells.

ABCA4 co-localizes with endo-phagolysosomal markers

To determine whether ABCA4 is expressed in the endo-phagolysosomal system, we tested for co-localization with endosomal and lysosomal markers in murine and human RPE. In distal retina sections from wild type albino mice (Balb/c) we observed co-localization of ABCA4 with lysosomal-associated membrane protein 1 (LAMP1) in the apical RPE but not in photoreceptor OS (Fig. 1.3C). As expected, LAMP1 but not ABCA4 immunofluorescence was seen in similar retina sections from albino *Abca4*$^{-/-}$ mice. In hfRPE cells, ABCA4 immunofluorescence was distributed in a granular pattern concentrated apically (Fig. 1.3D). The distribution of ABCA4 largely overlapped with that of caveolin-1 (CAV1) (Fig. 1.3D). CAV1 is a marker for endosomes and phagolysosomes[28]. These results suggest that ABCA4 is present in endo-phagolysosomal membranes of RPE cells.

iii. Materials and methods

Animals: All experiments were performed in accordance with the ARVO Statement for the Use of Animals in Ophthalmic and Vision Research and IACUC guidelines. Animals were housed in normal cyclic 12-hour light/12-hour dark conditions and fed *ad libitum*. All animals were homozygous for the *Rpe65* Leu450 variant and free of the retinal degeneration 8 (*rd8*) mutation in the crumbs homolog 1 (*Crb1*) gene. Wild type 129/Sv, pigmented *Mertk*$^{-/-}$ mice, and pigmented *Abca4*$^{-/-}$ mice were used for RPE-ABCA4 expression studies.

RNA-Seq analysis: For bovine RPE cell RNA-Seq analysis, bovine eyes were obtained from a local slaughterhouse (J W Treuth and Sons, Catonsville, MD) and processed the day of arrival. The eyes were rinsed in 70% ethanol to sterilize the external tissues. Total RNA was isolated from the native bovine RPE using miRNeasy Mini Kit (Qiagen, Valencia, CA). The total RNA

samples were submitted to Expression Analysis, Inc., for RNA-Seq analysis (Q^2 Solutions, Morrisville, NC). Briefly, stranded and rRNA depleted cDNA libraries were prepared from total RNA samples using the TruSeq Stranded mRNA Sample Prep Kit (Illumina, San Diego, CA). The cDNA libraries were analyzed for size distribution using an Agilent Bioanalyzer (Agilent, Santa Clara, CA), and then normalized to 2 nM using the KAPA Library Quantification Kit (#KK4824, KAPA Biosystems, Wilmington, MA). The libraries were sequenced using a 2x50 bp paired end protocol with the median number of 87.3 million reads across all samples on the Illumina HiSeq 2500 (Illumina). Following sequencing, base call files were converted into FASTQ files using Illumina Software (CASAVA) and Expression Analysis developed open source programs. To prepare the reads for alignment, the sequencing adapters and other low quality bases were clipped. Gene read counts, derived from three biologic replicates, were averaged and subjected to paired Student t-test analysis. Expression levels are given as gene counts and are normalized for variation between sequencing runs. The basic statistical calculations were performed using GraphPad Prism version 7.00 for Windows (GraphPad Software, La Jolla, CA). Names of human orthologs of the bovine dataset were obtained from the BioMart utility of Ensembl (http://www.ensembl.org/biomart/) or the HUGO Gene Nomenclature Committee (HGNC) Comparison of Orthology Predictions (HCOP) tool (http://www.genenames.org/cgi-bin/hcop). For hfRPE cell RNA-Seq analysis, methods have been described previously[21], and data can be accessed through the Gene Expression Omnibus (GEO: GSE67899).

Quantitative real-time polymerase chain reaction (qRT-PCR): Mouse retina and RPE were dissected from euthanized animals, and total RNA was extracted using Absolutely RNA Miniprep (Stratagene, La Jolla, CA) with DNAase treatment. RNA was reverse transcribed to cDNA using SuperScript III First Strand Synthesis (Invitrogen, Carlsbad, CA). Reactions for

qRT-PCR were set up with iTaq Universal SYBR Green Supermix (Invitrogen) and gene specific primer sets for mouse *Abca4* (Forward AGG GAG AGC TGT GGT TCT CA; Reverse AGC AAG TCG TCC TTT GGA GA), human *ABCA4* (Forward CCT GGA TGG GGA TGT AAA TG; Reverse GGC ATA TGC TCT GTG CTT GA), and human *RHO* (Forward AGA ATG GGG CAC ACA GTA GG; Reverse GGG ATC TGG GAT TTC CAT TT). Relative mRNA expression was calculated based on normalization to 18S RNA.

RPE Cell Culture and Immunocytochemistry: Detailed protocol of hfRPE cell culture has been previously described[27,29]. Briefly, RPE cells were collected from 18- to 23-week-old aborted fetuses (Advanced Bioscience Resources, Alameda, CA) then grown and maintained in Chee's essential replacement medium containing 1% calf serum and minimal essential medium containing 1.8 mM $CaCl_2$ (Sigma-Aldrich, St. Louis, MO) for two months before use. Human RPE cells with their associated filters were fixed in 4% formaldehyde/0.1M phosphate buffer for 30 minutes, embedded in agarose (TypeXI low gelling temperature, Sigma-Aldrich), and cut into 100 μm sections on a VT1000S vibratome (Leica Microsystems, Wetzlar, Gemany). The sections were blocked with 0.5% goat serum and 1% BSA in PBS for one hour followed by incubation with rabbit anti-ABCA4 (1:100, ab72955, Abcam), goat anti-caveolin 1 (1:100, ab36152, Abcam), or mouse anti-rhodopsin (RHO1D4; 1:250, University of British Columbia) separately. The sections were rinsed three times and incubated in secondary antibodies conjugated with Alexa Fluor dyes (goat anti-rabbit IgG-647, goat anti-mouse IgG-647, or donkey anti-goat IgG-594; 1:500, Invitrogen) for one hour. The sections were stained with DAPI nuclear marker (Invitrogen), mounted with 5% n-propyl gallate in 100% glycerol, and imaged with an Olympus FluoView FV1000 confocal laser-scanning microscope (Waltham, MA) under a 60x oil objective.

Immunoblotting: Retina and RPE were dissected from mouse eyecups and subsequently homogenized in PBS with Halt Protease Inhibitor cocktail (Life Technologies, Carlsbad, CA). Protein samples were treated with Benzonase nuclease (Sigma-Aldrich) at room temperature for one hour and re-homogenzied with 1% SDS. Upon centrifugation of samples at 3,000x g for 10 minutes, cell debris was pelleted out and the supernatant containing protein was collected. Protein concentrations were measured using the MicroBCA assay kit (ThermoFisher, Canoga Park, CA), and samples were fractionated on 4-12% Bis-Tris gels (Invitrogen). Membranes were blocked with Odyssey blocking buffer (LI-COR Biosciences, Lincoln, NE) followed by incubation in primary antibody overnight at 4°C (goat anti-ABCA4, 1:200, sc-21460, Santa Cruz) or for one hour at room temperature (mouse anti-α-tubulin, 1:100, T9026, Sigma-Aldrich; rabbit anti-RDS/peripherin custom anti-sera, 1:200[30]). Membranes were washed with PBS-Tween, probed for one hour at room temperature with cognate IR-dye labeled secondary antibodies from LI-COR, and imaged with the CLx Odyssey system (LI-COR).

Immunohistochemistry: Mouse eyes were fixed in 2% paraformaldehyde/0.1M sodium phosphate buffer for one hour followed by preparation of eyecups, which were then infiltrated with 10-30% sucrose for cryoprotection. Eyecups were embedded in cryo-OCT (Tissue-Tek) and cut into 8 µm sections. Slides were blocked with normal goat or donkey serum and probed overnight at 4°C with rabbit anti-ABCA4 (1:1,000, ab72955, Abcam), mouse anti-LAMP1 (1:100, ab25630, Abcam), and goat anti-caveolin 1 (1:100, ab36152, Abcam) primary antibodies. Slides were washed and labeled with conjugated Alexa Fluor secondary antibodies for 1 hour at room temperature. All mouse primary antibodies were used in conjunction with the Mouse-on-Mouse Immunodetection Kit (Vector Labs, Burlingame, CA). Images were obtained with the Olympus FV1000 confocal microscope using a 60x objective.

iv. Figures

A. RNA-Seq analysis of bovine and human RPE

Gene	Bovine RPE RNA-Seq Expression	hfRPE RNA-Seq Expression
ABCA4	**9463**	**46**
RHO	**85**	**0**
OPN1LW	0	0
OPN1SW	2	0
OPN4	0	0
RPE65	**1094010**	**280**
BEST1	408894	2108
LRAT	130197	542

B. qRT-PCR of hfRPE and human retina

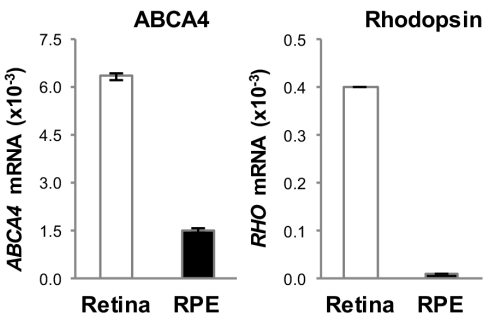

Figure 1.1. *ABCA4* RNA is expressed in bovine RPE and in hfRPE cells. (A) RNA-Seq analysis of bovine RPE and cultured hfRPE cells shows elevated *ABCA4* (red font) along with elevated *RPE65* and other RPE-specific genes (black font) despite negligible levels of *RHO* and other retina-specific genes (blue font). **(B)** ABCA4 and Rhodopsin mRNA levels by qRT-PCR, normalized to 18S, from hfRPE cells are shown (black bars). Retina controls represent mRNA from human donor cadavers (white bars). For hfRPE cells, each experiment was repeated three times from three different donor cell lines.

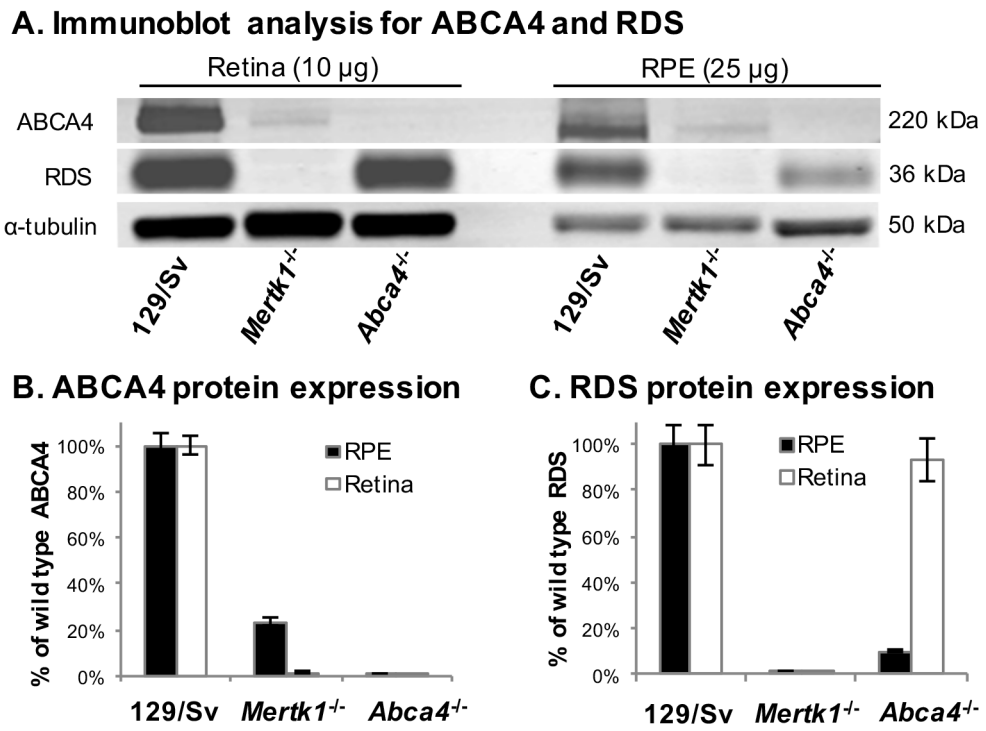

Figure 1.2. ABCA4 protein is expressed in the RPE of *Mertk1*$^{-/-}$ mice. (A) Representative immunoblots for ABCA4, RDS/Peripherin, and α-tubulin from retina and RPE protein homogenates, for which 10 and 25 µg of protein was loaded per lane, respectively. ABCA4 **(B)** and RDS/Peripherin **(C)** protein levels, normalized to α-tubulin, are represented as a relative percent of wild type 129/Sv levels, in 5-month-old pigmented mice. Data presented as mean ± S.D. (n=3 mice per group).

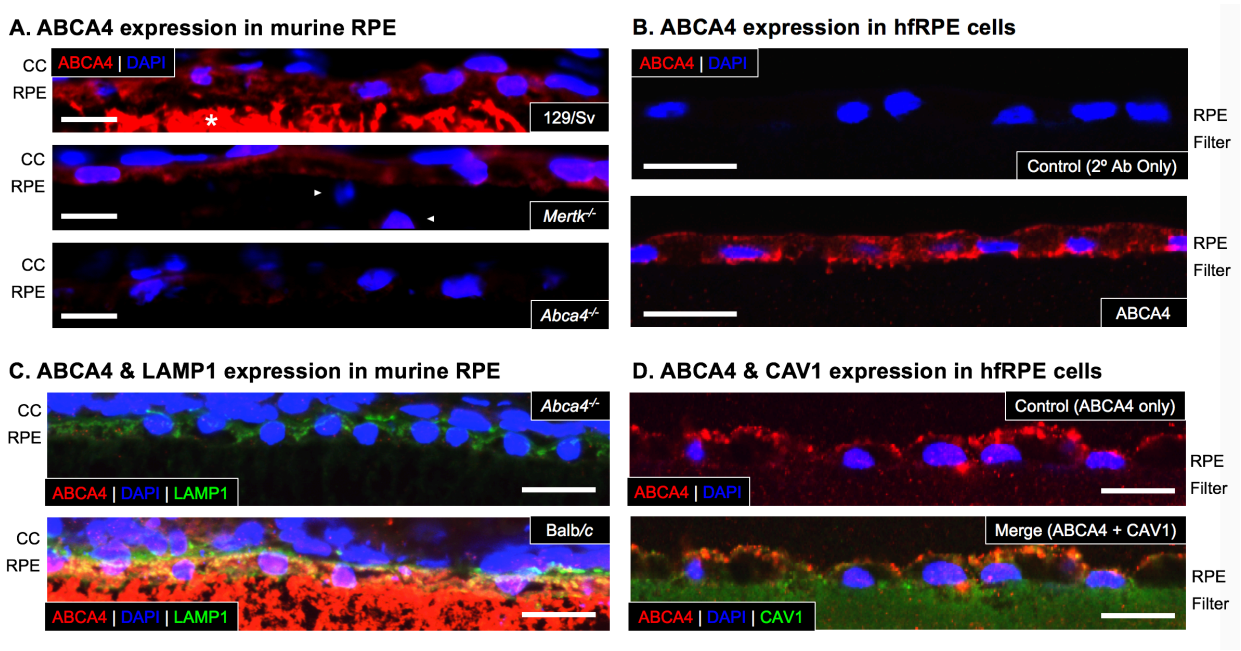

Figure 1.3. Immunohistochemical expression of ABCA4 in the RPE demonstrates co-localization with lysosomal LAMP1 and endo-phagolysosomal CAV1. (A) Representative confocal images of murine retinal sections showing strong ABCA4 (red) immunoreactivity in wild type (top panel) and *Mertk*$^{-/-}$ (middle panel) RPE but near absent ABCA4 expression in *Abca4*$^{-/-}$ RPE (bottom panel); asterisk (*) denotes photoreceptor outer segments; arrowheads (▷) denote rare photoreceptor outer nuclei displaced due to the complete loss of photoreceptor outer segments. **(B)** ABCA4 (red) immunoreactivity is seen in the representative confocal image of a hfRPE cell culture section stained for ABCA4 (bottom panel), in contrast with the secondary antibody control (top panel). **(C)** Representative confocal image of a retinal section shows strong lysosome-associated membrane protein (LAMP1, green) immunoreactivity in the RPE of 2-month-old albino *Abca4*$^{-/-}$ mice (top panel) with negligible ABCA4 (red) expression; corresponding image of age-matched wild type Balb/*c* mice (bottom panel) with ABCA4 expression throughout the RPE and retina reveals that LAMP1 co-localizes with ABCA4 in the RPE, but not in photoreceptor outer segments. **(D)** Representative confocal image of a hfRPE cell culture section, where ABCA4 (red) immunoreactivity is seen diffusely throughout the RPE cells (top panel, Control); when co-stained with endosomal caveolin 1 (CAV1, green), ABCA4 (red) co-localizes with structures that also express CAV1 in hfRPE cell culture sections (bottom panel, Merge). The green labeling of the filter in the CAV1 panel is due to nitrocellulose autofluorescence with 488-nm excitation[31]. Nuclei stained with DAPI (blue); 60x objective; scale bar = 10 μm. For murine RPE sections, three independent animals were analyzed per group. For hfRPE cells, each experiment was repeated three times with three different donor cell lines.

Chapter 2: The functional role of RPE-expressed ABCA4

i. Introduction

Stargardt disease and the Abca4$^{-/-}$ mouse model

Recessive Stargardt macular degeneration (STGD1) is a blinding disease of children and young adults caused by mutations in the *ABCA4* gene[15,17]. Both recessive Stargardt disease (STGD1) patients and mice with a null mutation in Abca4 (*Abca4*$^{-/-}$) show accelerated deposition of lipofuscin granules, or "age pigment," in the RPE, which precedes photoreceptor death[12,32-39]. Lipofuscin refers to the autofluorescent, intracellular lipid material found with increasing age in many post-mitotic cells of the body[40,41]. The chemical make-up and electron microscopic appearance of lipofuscin found in the RPE is distinct from that of other organs, in that it includes a large amount of vitamin A derivatives[42-44]. The major fluorophore of lipofuscin in RPE cells is the bisretinoid pyridinium salt, *N*-retinylidene-*N*-retinylethanolamine (A2E), which forms by condensation of a second all-*trans*-RAL with *N*-ret-PE[33,45-48]. A notable feature of the *Abca4*$^{-/-}$ mouse that consistently recapitulates STGD1 is the accumulation of lipofuscin containing A2E in the RPE[12,49-51]. Several mechanisms of cytotoxicity from A2E accumulation in the RPE, including cellular oxidative stress and complement dysregulation, result in RPE failure and subsequent photoreceptor loss[52-64].

Mechanism of RPE bisretinoid accumulation associated with ABCA4 loss

Daily circadian phagocytosis of distal OS by the adjacent RPE[23,24] accounts for the deposition of photoreceptor-derived bisretinoid precursors in the RPE[65-67]. It was previously thought that bisretinoid formation was dependent on the availability of all-*trans*-RAL produced in photoreceptor OS only. If ABCA4 was indeed *only* expressed in OS disc membranes,

accumulation of bisretinoids should be seen in cyclic light-raised *Abca4*$^{-/-}$ RPE, but not in dark-reared *Abca4*$^{-/-}$ RPE, because photoisomerization of rhodopsin and subsequent release of all-*trans*-RAL does not occur in the dark. However, it was shown that dark-reared *Abca4*$^{-/-}$ mice *do* accumulate bisretinoids (A2E and iso-A2E) in the RPE at rates similar to cyclic-light reared mice[50], suggesting that retinaldehydes in the RPE, locally released from phagolysosomes, may be forming bisretinoids directly in the RPE. The authors of this study assume that bisretinoids are still being formed in photoreceptors, but attribute 'dark-reared' bisretinoid formation to 11-*cis*-RAL, vs. all-*trans*-RAL, as the primary substrate. However, given the very high stability of rhodopsin in the dark, any 11-*cis*-RAL in the photoreceptors would presumably be sequestered immediately by apo-opsin[68], and so an alternative explanation for 'dark-reared' bisretinoids could be that they are formed directly in the RPE. The possibility for RPE-derived bisretinoids is highly plausible, given our finding of endogenous RPE-expressed ABCA4, demonstrated in Chapter 1.

Given the various biochemical and clinical differences seen between wild type and *Abca4*$^{-/-}$ mice, we sought to determine if replacing ABCA4 specifically in the RPE of *Abca4*$^{-/-}$ mice would alter the phenotype and thus uncover a functional role for RPE-expressed ABCA4. The transgenic *RPE-Abca4-Tg/Abca4*$^{-/-}$ mouse line was generated on the *Abca4*$^{-/-}$ background to express ABCA4 in RPE cells, but not in photoreceptors. Chapter 2 of this work suggests that RPE-expressed ABCA4 plays a similar role to that of ABCA4 expressed in photoreceptors, that is, to help clear free retinaldehyde by flipping *N*-ret-PE to the cytoplasm, thereby preventing the buildup of potentially toxic bisretinoids. (Fig. 2.1)

ii. Characterization of a transgenic mouse with selective expression of ABCA4 in the RPE

Abca4 is uniquely expressed in the RPE of the RPE-Abca4-Tg/Abca4$^{-/-}$ *mouse*

Using a construct containing the normal mouse *Abca4* coding region downstream of the RPE-specific *Rpe65* promoter (Fig. 2.2), we generated several transgenic lines on the *Abca4*$^{-/-}$ background and then selected one line, *RPE-Abca4-Tg/Abca4*$^{-/-}$*,* with highest expression of ABCA4 in the RPE and, correspondingly, lowest expression of ABCA4 in the retina. The level of RPE-expressed ABCA4, normalized to tubulin, in 6-month-old *RPE-Abca4-Tg/Abca4*$^{-/-}$ transgenic mice was about 25% of wild type levels (Fig. 2.3A-B). In contrast, the protein level of ABCA4 in the corresponding retinas of *RPE-Abca4-Tg/Abca4*$^{-/-}$ transgenic mice was less than 5% that of wild type retina. *RPE-Abca4-Tg/Abca4*$^{-/-}$ transgenic mice expressed approximately 50% of wild type *Abca4* mRNA levels, normalized to 18S, in the RPE at three months of age (Fig. 2.3C). In contrast, less than 10% of wild type *Abca4* mRNA levels were found in the corresponding retinas of *RPE-Abca4-Tg/Abca4*$^{-/-}$ mice. Non-transgenic control littermates of *RPE-Abca4-Tg/Abca4*$^{-/-}$ are genetically equivalent to *Abca4*$^{-/-}$ mice, and therefore expressed 0% of wild type *Abca4* mRNA. Finally, retina sections from 1-year-old mice stained with anti-Rim 3F4 ABCA4 demonstrate strong RPE-expressed ABCA4 in Balb/*c* wild type mice by immunohistochemistry (Fig. 2.3D). Whereas ABCA4 expression is likewise strong in the RPE of *RPE-Abca4-Tg/Abca4*$^{-/-}$ transgenic mice, it is notably absent in the RPE of non-transgenic control *Abca4*$^{-/-}$ littermates.

RPE-Abca4-Tg/Abca4$^{-/-}$ *mice show rescue of bisretinoid accumulation, autofluorescence, and lipofuscin burden seen in Abca4*$^{-/-}$ *mice*

To determine whether RPE-expressed ABCA4 might play a functional role to prevent bisretinoid accumulation in RPE cells, we compared levels of several lipofuscin fluorophores in the retina and RPE of 3-month-old wild type, *Abca4*$^{-/-}$, and *RPE-Abca4-Tg/Abca4*$^{-/-}$ mice by high performance liquid chromatography (HPLC). Levels of A2E in the RPE were reduced by approximately 50% in *RPE-Abca4-Tg/Abca4*$^{-/-}$ versus *Abca4*$^{-/-}$ mice (Tukey's $p<0.0001$; ANOVA

F-ratio = 113.0, $p<0.0001$), although the levels of these pigments were still higher in the *RPE-Abca4-Tg/Abca4*$^{-/-}$ versus wild type mice (Tukey's $p=0.0002$) (Fig. 2.4A-D). Likewise, levels of A2PE, all-*trans*-RAL Dimer-PE, and A2PE-H_2 all trended lower in the RPE of *RPE-Abca4-Tg/Abca4*$^{-/-}$ versus *Abca4*$^{-/-}$ mice, although not as low as Balb/*c*. Interestingly, the levels of lipofuscin fluorophores were similar in *RPE-Abca4-Tg/Abca4*$^{-/-}$ versus *Abca4*$^{-/-}$ retinas, consistent with non-rescue of the phenotype in photoreceptors.

By confocal microscopy of RPE flat mounts, we also observed that RPE of *RPE-Abca4-Tg/Abca4*$^{-/-}$ mice had approximately 25% lower autofluorescence (at 488 nm excitation with a 500-545 nm emission filter) compared to that of *Abca4*$^{-/-}$ littermates (Tukey's $p=0.0006$; ANOVA F-ratio = 37.2, $p<0.0001$), at levels still greater than wild type mice (Tukey's $p<0.0001$) (Fig. 2.5A-B). Finally, fractional lipofuscin granules per 100 μm^2 RPE area in electron microscopy (EM) sections from *RPE-Abca4-Tg/Abca4*$^{-/-}$ mice (8.6%) were approximately half of that seen in the non-transgenic *Abca4*$^{-/-}$ control littermates (15.8%) (Fig. 2.5C-D) (Tukey's $p=0.0186$; ANOVA F-ratio 14.4; $p=0.0016$) but still higher than the 3% fractional lipofuscin granule burden observed in the Balb/*c* wild type controls (Tukey's $p=0.0951$).

Morphologic and biochemical retinal preservation is seen in the RPE-Abca4-Tg/Abca4$^{-/-}$ *transgenic mouse*

An important feature of the *Abca4*$^{-/-}$ phenotype is slow degeneration of photoreceptors, which leads to visual loss in STGD1 patients. Here we tested whether expression of ABCA4 in RPE cells affects photoreceptor degeneration in *Abca4*$^{-/-}$ mice. Photoreceptor degeneration can be quantitated by counting photoreceptor nuclei in the outer nuclear layer (ONL) of retina sections. In order to further assess the phenotypic impact of RPE-expressed ABCA4, we analyzed retinal morphology of 1-year-old eyes embedded in plastic. Compared to wild type, one-year-old non-transgenic *Abca4*$^{-/-}$ mice exhibited a 20% reduction in photoreceptor nuclei

(Fig. 2.6A-B) (Tukey's $p < 0.0001$). In contrast, *RPE-Abca4-Tg/Abca4*$^{-/-}$ littermates exhibited only 10% loss of photoreceptors compared to wild type mice (Fig. 2.6A-B) (Tukey's $p = 0.0061$; ANOVA F-ratio 14.8, $p < 0.0001$). Expression of ABCA4 in RPE cells therefore slowed the photoreceptor degeneration seen in *Abca4*$^{-/-}$ mice by a factor of two.

Likewise, 11-*cis*-retinaldehyde (11-*cis*-RAL) levels by HPLC were significantly lower in the RPE of non-transgenic *Abca4*$^{-/-}$ mice compared with wild type mice (Tukey's p=0.0220; ANOVA F-ratio = 4.7, p=0.0235), while there was a non-statistically significant increase in 11-*cis*-RAL levels in the RPE of *RPE-Abca4-Tg/Abca4*$^{-/-}$ mice compared with *Abca4*$^{-/-}$ mice (Fig. 2.6C-D) (Tukey's p=0.6455).

To evaluate retinal function, we evaluated dark-adapted *a*- and *b*-wave ERG responses at one year of age. One-way ANOVA testing (F-ratio = 4.1654, p=0.0364) with Tukey-Kramer post-hoc analysis revealed that Balb/*c* mice trended to have significantly larger scotopic *a*-wave maximum amplitudes than the *RPE-Abca4-Tg/Abca4*$^{-/-}$ (p=0.0717) and *Abca4*$^{-/-}$ (p=0.0544) lines (Fig. 2.7A-B). However, both of these groups of mice on the *Abca4*$^{-/-}$ background, were not statistically different (0.9569). Group-wise comparison of scotopic *b*-wave maximum amplitudes revealed no significant differences between Balb/*c*, *RPE-Abca4-Tg/Abca4*$^{-/-}$, or *Abca4*$^{-/-}$ mouse lines.)

Complement dysregulation seen in the Abca4$^{-/-}$ *mouse is improved in the RPE-Abca4-Tg/Abca4*$^{-/-}$ *transgenic mouse*

Several studies have suggested that the cellular pathogenesis of ABCA4-mediated maculopathy involves complement dysregulation and cellular oxidative stress[52,69-71]. To further investigate the role of these pathogenic mechanisms in the etiology of the *Abca4*$^{-/-}$ mouse, we measured RPE levels of the complement activation product C3b in 6-month-old mice. Compared to wild type RPE, *Abca4*$^{-/-}$ RPE have significantly greater levels of C3b accumulation

(Tukey's p=0.0369; ANOVA F-ratio = 5.6644, p=0.0415). RPE from *RPE-Abca4-Tg/Abca4*$^{-/-}$ transgenic mice, on the other hand, show reduced levels of C3b (Tukey's p=0.5108) compared with *Abca4*$^{-/-}$ mice (Fig. 2.8A-B).

iii. Materials and methods

Animals: All experiments were performed in accordance with the ARVO Statement for the Use of Animals in Ophthalmic and Vision Research and IACUC guidelines. Animals were housed in normal cyclic 12-hour light/12-hour dark conditions and fed *ad libitum*. All animals were homozygous for the *Rpe65* Leu450 variant and free of the *rd8* mutation in the *Crb1* gene. Transgenic mice expressing ABCA4 in the RPE on the albino *Abca4*$^{-/-}$ background (*RPE-Abca4-Tg*/*Abca4*$^{-/-}$) were used with albino non-transgenic *Abca4*$^{-/-}$ littermate and albino wild type (Balb/*c*) age-matched controls.

Generation of RPE-Abca4-Tg/*Abca4*$^{-/-}$ *transgenic mice:* We generated a transgenic construct (RPE-Abca4), containing the normal mouse *Abca4* coding region downstream of the RPE-specific RPE65 promoter in the transgene plasmid, pSTEC-1 (Fig. 2.2). A 700 bp 5' untranslated region of the *Rpe65* gene corresponding to the *Rpe65* promoter[72] was PCR amplified from pTR4 plasmid and subcloned into HindIII (5') and PstI (3') restriction sites of the pSTEC-1 vector[73] to increase transgene expression level by including a spliceable intron. The *Rpe65* promoter/Intron 1 complex was then cloned into the 5' end of the *Abca4* cDNA in the pSport-Abca4 plasmid using EcoRI (5') and SalI (3') restriction sites. The entire transgene (*Rpe65*-intron-*Abca4*) was excised from the pSport6-Abca4 using EcoRI restriction sites. RPE-specific *Rpe65* promoter (RPE-Abca4). The RPE-Abca4 construct was sent to the UCLA Transgenic Core facility for injection and resulted in six lines of transgenic mice. Each line was

crossed onto the albino *Abca4*$^{-/-}$ background and one line was identified to have the most robust RPE-specific expression of *Abca4* by qRT-PCR, immunoblotting, and immunocytochemistry. Primers used for genotyping *Rpe65-Abca4-Tg*/*Abca4*$^{-/-}$ mice included: Forward AGG AAA AGG CAG AAG ATT CGC TTT GTA G; Reverse: TGG GAA AAT GGC ATT CAT GCT GAC.

Quantitative real-time polymerase chain reaction (qRT-PCR): Mouse retina and RPE/eyecups were dissected from euthanized animals, and total RNA was extracted using Absolutely RNA Miniprep (Stratagene, La Jolla, CA) with DNAase treatment. RNA was reverse transcribed to cDNA using SuperScript III First Strand Synthesis (Invitrogen, Carlsbad, CA). Reactions for qRT-PCR were set up with iTaq Universal SYBR Green Supermix (Invitrogen) and gene specific primer sets for mouse *Abca4*: Forward AGG GAG AGC TGT GGT TCT CA; Reverse AGC AAG TCG TCC TTT GGA GA. Relative mRNA expression was calculated based on normalization to 18S RNA.

Immunoblotting: Retina and RPE were dissected from mouse eyecups and subsequently homogenized in PBS with Halt Protease Inhibitor cocktail (Life Technologies, Carlsbad, CA). Protein samples were treated with Benzonase nuclease (Sigma-Aldrich) at room temperature for one hour and re-homogenzied with 1% SDS. Upon centrifugation of samples at 3,000x g for 10 minutes, cell debris was pelleted out and the supernatant containing protein was collected. Protein concentrations were measured using the MicroBCA assay kit (ThermoFisher, Canoga Park, CA), and samples were fractionated on 4-12% Bis-Tris (ABCA4, GAPDH, α-tubulin) or 4-8% Tris Acetate (C3b) gels (Invitrogen). Membranes were blocked with Odyssey blocking buffer (LI-COR Biosciences, Lincoln, NE) followed by incubation in primary antibody overnight at 4°C (goat anti-ABCA4, 1:200, sc-21460, Santa Cruz; goat anti-C3, 1:100, 0855444, MP Biomedicals) or for one hour at room temperature (mouse anti-α-tubulin, 1:100, T9026, Sigma-

Aldrich; rabbit anti-GAPDH, 1:500, sc-25778, Santa Cruz). Membranes were washed with PBS-Tween, probed for one hour at room temperature with cognate IR-dye labeled secondary antibodies from LI-COR, and imaged with the CLx Odyssey system (LI-COR).

Immunohistochemistry: Mouse eyes were fixed in 2% paraformaldehyde/0.1M sodium phosphate buffer for one hour followed by preparation of eyecups, which were then infiltrated with 10-30% sucrose for cryoprotection. Eyecups were embedded in cryo-OCT (Tissue-Tek) and cut into 8 µm thick sections. Slides were blocked with normal goat or donkey serum and probed overnight at 4°C with rabbit anti-ABCA4 (1:1000, ab72955, Abcam) primary antibody. Slides were washed and labeled with conjugated Alexa Fluor secondary antibody for 1 hour at room temperature. Images were obtained with the Olympus FV1000 confocal microscope using a 60x objective.

Quantitation of A2E in mouse eyes: Bisretinoids were isolated by chloroform extraction followed by analysis using high performance liquid chromatography (HPLC), as described previously[52]. Briefly, retina and RPE samples previously stored at -80°C were homogenized in 1x PBS, washed with chloroform/methanol (2:1, v/v), and extracted with chloroform/water (4:3, v/v). The organic phase was isolated after centrifugation at 1,000x g for 10 minutes, then dried down under argon and resuspended in 100 µl of isopropanol.

RPE Flat Mount: Eyes of 6-month-old mice were enucleated, fixed in 2% paraformaldehyde/0.1M sodium phosphate buffer ($NaPO_4$, pH 7.4) for thirty minutes at room temperature, thrice rinsed and dissected in 0.1M $NaPO_4$ to create RPE-choroid-scleral eyecups with the neurosensory retina and anterior segment removed. To flatten eyecups, eight leaflets were made with straight cuts using Castroviejo microdissecting scissors. Resultant RPE-

choroid-scleral flat mounts were permeabilized with 1% Triton X-100, blocked with 1% BSA/5% NGS and incubated at 4°C overnight with rabbit anti-ZO-1 (ThermoFisher). Flat mounts were mounted with ProLong Gold anti-fade with DAPI (Molecular Probes), and imaged with an Olympus confocal microscope using a 60x objective lens. Autofluorescence was detected by excitation with 488 nm (Argon) laser using a 500-545 nm emission filter, and images were quantified in ImageJ.

Light and Electron Microscopy: Mice were anesthetized with isofluorane and fixed by intracardiac perfusion with 2% formaldehyde and 2.5% glutaraldehyde in 0.1M sodium phosphate buffer, pH 7.2. The nasal and temporal hemispheres of each eyecup were separated and fixed in 1% osmium tetroxide dissolved in 0.1M sodium phosphate buffer, then dehydrated in a graded series of alcohols. The temporal hemispheres were embedded in an Epon/Araldite mixture (5:3 part) for light microscopy, whereas the nasal hemispheres were cut into quadrants and embedded in Araldite 502 (Tousimis Research Corporation and Electron Microscope Sciences) for EM. Sections of 1 μm thickness for light microscopy were cut on a Leica Ultracut microtome and stained with Toluidine blue. 300 x 300 dpi images were obtained with a CoolSNAP digital camera (Photometrics, Tucson, AZ) affixed to Zeiss Axiophot microscope (Thornwood, NY) with a 63X oil immersion objective (n=10-20 animals per group). The total number of photoreceptor nuclei in three adjacent mid-peripheral visual field locations were averaged per eye and plotted in Microsoft Excel. Ultrathin sections for EM were cut on a Leica Ultracut microtome and collected on 200-mesh copper grids. Sections were stained with uranium and lead salts prior to viewing on a JEM 1200-EX electron microscope (JEOL, Peabody, MA). At least ten 100 μm^2 adjacent EM images were acquired from the superior region of each eye at 15000x. From each image, using Soft-imaging software (Olympus Soft Imaging Solutions, EMSIS, GmbH, Münster, Germany), fractional lipofuscin granules were

measured by obtaining the area in μm^2 occupied by lipofuscin over the area in μm^2 occupied by cytoplasm. One eye from each animal was included, and ten images from each eye were averaged, such that each animal's fractional lipofuscin granule measurement and Bruch's membrane measurement corresponded to an average of at least ten adjacent EM images from one eye (n=5-9 animals per group).

Electroretinography: Mice were dark-adapted overnight and anesthetized with intraperitoneal ketamine (15 µg/gm) and xylazine (5 µg/gm). ERGs were recorded from the corneal surface of both eyes using a gold loop electrode referenced to a gold wire in the mouth. Eyes were dilated with 1% atropine sulfate and lubricated with 2.5% methylcellulose. Body temperature was maintained at 38°C with a heated water pad. Mice were positioned in front of the anterior opening of a large dome with an interior surface of highly reflective white matte paint (Eastman Kodak Corporation #6080). Light was generated with a photic stimulator (Grass Instruments, PS33 Plus) affixed to the outside of the dome at 90º to the viewing porthole. Responses were amplified (Grass CP511 AC amplifier, x10,000) and digitized using an I/O board (National Instruments, PCI-1200) in a personal computer. Signal processing was performed with custom software. Rod mediated responses were recorded to blue (Wratten 47A; λ_{max} = 470 nm) flashes of light over a 4.0 log unit range of intensities (in 0.3 log unit steps) up to the maximum allowable by the photic stimulator (0.35 cd/m^2). Cone responses were obtained with white flashes on the rod-saturating background (32.0 cd/m^2) after ten minutes of exposure to the background light.

Statistical analysis: The results were presented as means with S.D. of a minimum of four to six animals per group unless otherwise specified. Two-group comparisons were performed using the Student's *t*-test in Microsoft Excel, whereas multiple group comparisons were performed

using the one-way analysis of variance (ANOVA) test with Tukey's post-hoc analysis in JMP Pro v12 (SAS Institute, Cary, NC).

iv. Figures

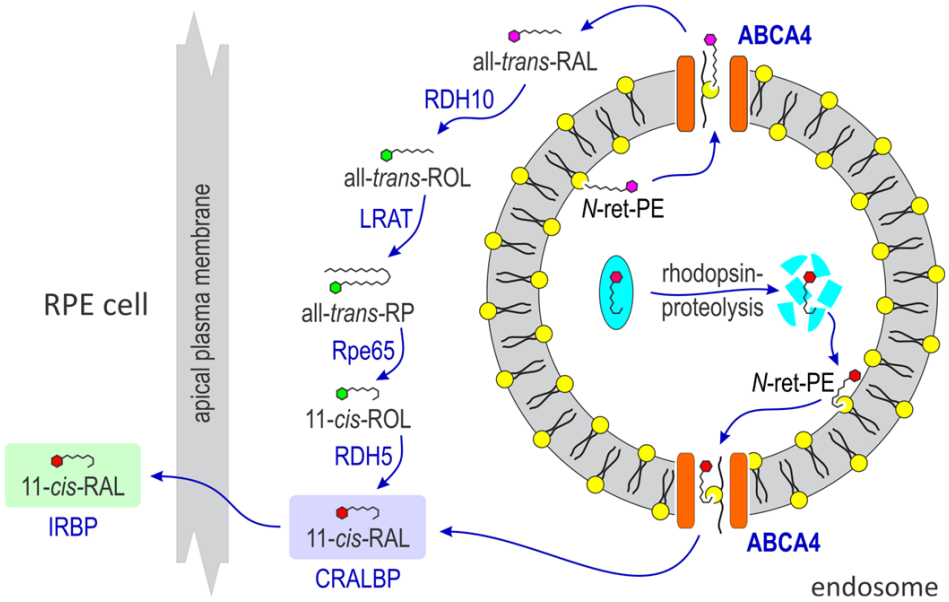

Figure 2.1. Proposed role of ABCA4 in the RPE. Following proteolysis of rhodopsin, 11-*cis*-RAL (red) is released and condenses with PE on the luminal face of RPE endo-phagolysosomal membranes to form 11-*cis*-*N*-ret-PE. A fraction of 11-*cis*-*N*-ret-PE may thermally isomerize to all-*trans*-*N*-ret-PE. ABCA4 in the RPE, expressed in the membrane of endosomes and lysosomes, flips either isomer of *N*-ret-PE from the luminal to cytoplasmic surface. Following its translocation to the RPE cytoplasm, spontaneous hydrolysis of *N*-ret-PE would then yield free 11-*cis*-RAL or all-*trans*-RAL, which would contribute to opsin pigment regeneration via either CRALBP-mediated export of 11-*cis*-RAL back to the photoreceptor, or retinol dehydrogenase type-10 (RHD10)-mediated reduction of all-*trans*-RAL to all-*trans*-retinol for recycling of visual pigment via conventional RPE visual cycle enzymes (i.e. LRAT, RPE65, RDH5).

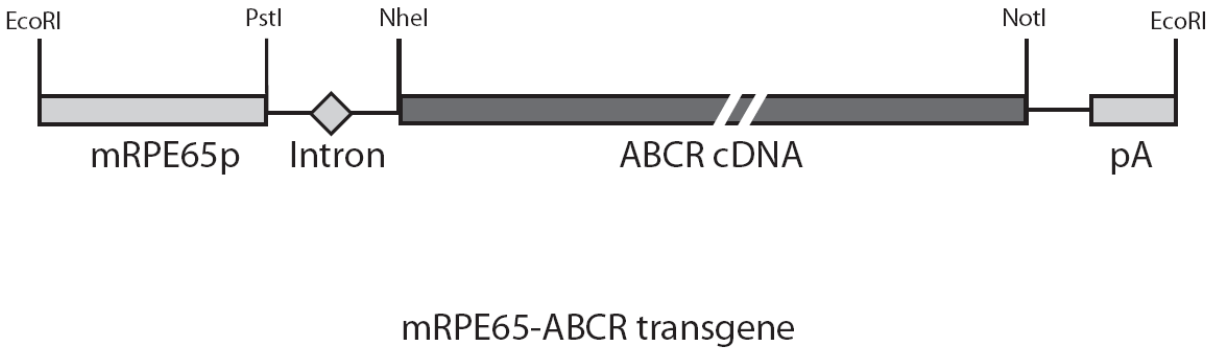

Figure 2.2. Schematic of mRPE65-ABCA4 transgene. The *RPE-Abca4-Tg*/*Abca4*$^{-/-}$ mouse was generated using a transgenic construct containing the normal mouse Abca4 coding region downstream of the RPE-specific RPE65 promoter.

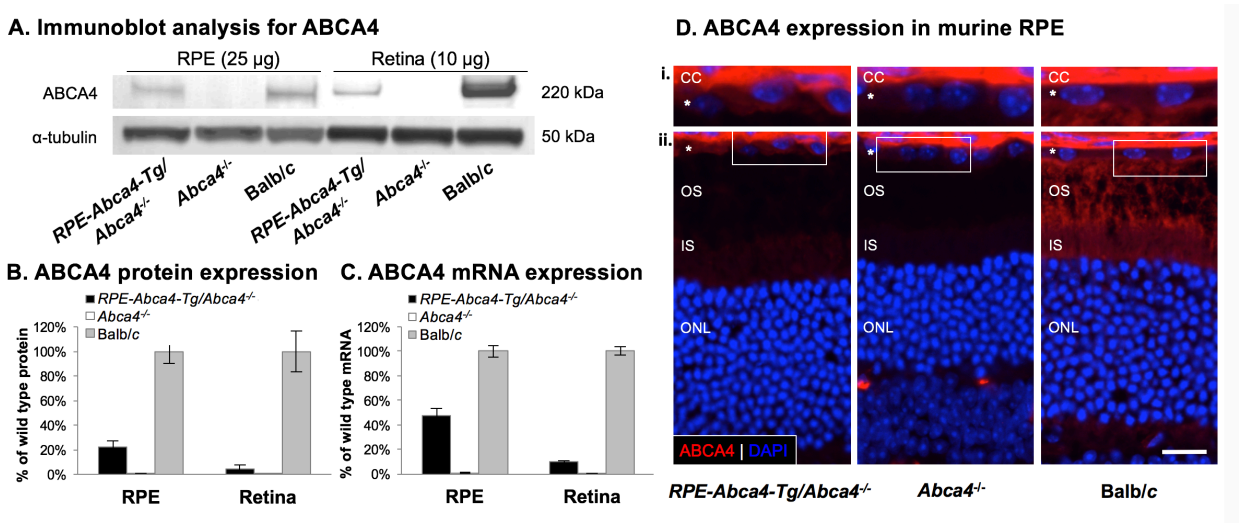

Figure 2.3. ABCA4 is expressed in the RPE of *RPE-Abca4-Tg/Abca4*$^{-/-}$ mice. (A) Representative immunoblot for ABCA4 and α-tubulin from retina and RPE homogenates, for which 10 and 25 µg of protein was loaded per lane, respectively. **(B)** Levels of ABCA4 protein by Western blot from 6-month-old albino *Abca4*$^{-/-}$ and *RPE-Abca4-Tg/Abca4*$^{-/-}$ mice, normalized to α-tubulin, are represented as a percent of wild type Balb/*c* levels (n=7 mice per group). **(C)** Levels of *Abca4* mRNA by qRT-PCR from 2-month-old albino *Abca4*$^{-/-}$ and *RPE-Abca4-Tg/Abca4*$^{-/-}$ mice, normalized to 18S, are represented as a percent of wild type Balb/*c* levels (n=7-11 mice per group). **(D)** Representative confocal images of retinal sections from *RPE-Abca4-Tg/Abca4*$^{-/-}$, *Abca4*$^{-/-}$, *and* Balb/*c* mice from 1-year-old mice show ABCA4 immunoreactivity (red) and DAPI nuclear staining (blue); upper row (i) represents zoom-in of boxed areas below (ii); asterisk (*) denotes RPE layer; CC = choriocapillaris; OS = outer segments; IS = inner segments; ONL = outer nuclear layer; 60x objective; scale bar = 10 µm.

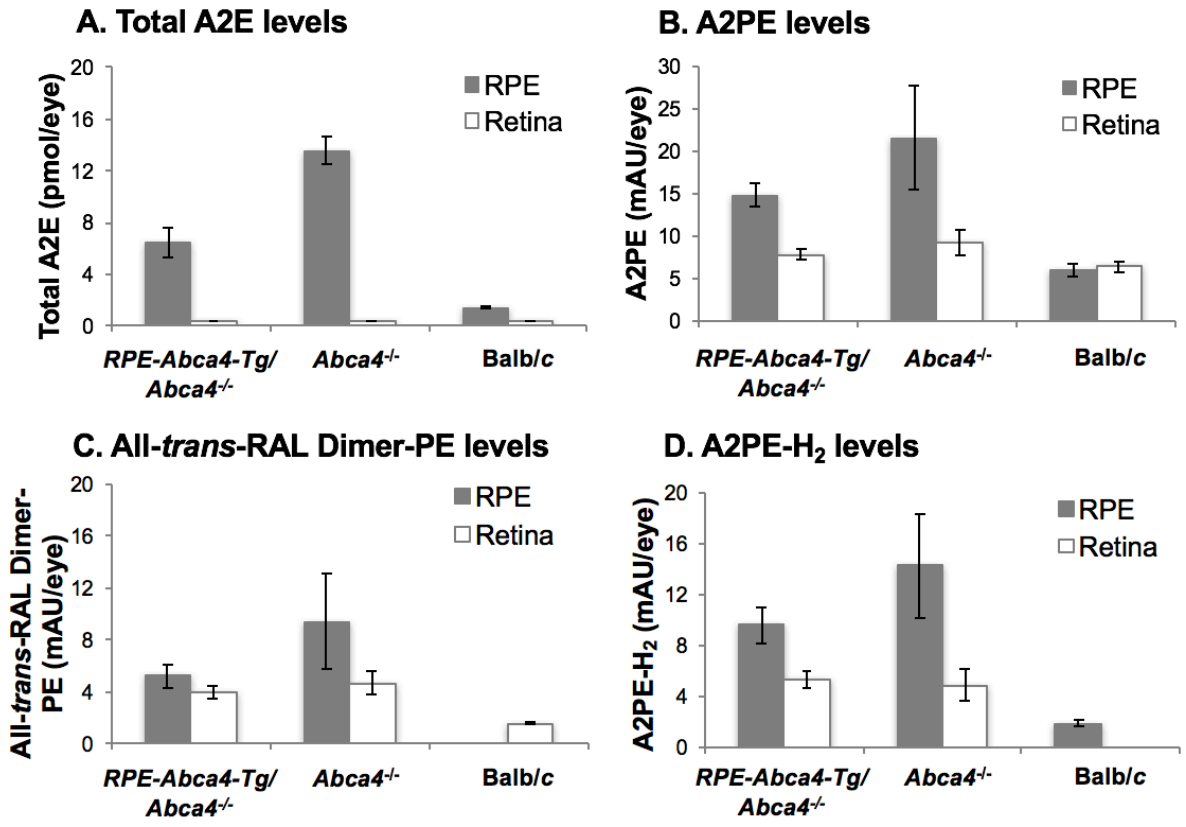

Figure 2.4. Bisretinoid levels are lower in the RPE of *RPE-Abca4-Tg/Abca4*$^{-/-}$ mice compared to the RPE of *Abca4*$^{-/-}$ mice. Total A2E **(A)**, A2PE **(B)**, All-*trans*-RAL Dimer-PE **(C)**, and A2PE-H_2 **(D)** levels are expressed as milliabsorbance units (mAU) per eye, whereas total A2E (A) represents sum of A2E and iso-A2E in picomoles (pmol) per eye. Absorption units corresponding to the A2E peak at 435 nm were converted to pmols using a calibration curve with an authentic A2E standard and the published molar extinction coefficient for A2E[74]. Bisretinoids were extracted from retina and RPE homogenates of 3-month-old albino mice and analyzed by normal phase HPLC. Data presented as mean ± S.D. (n=5 mice per group).

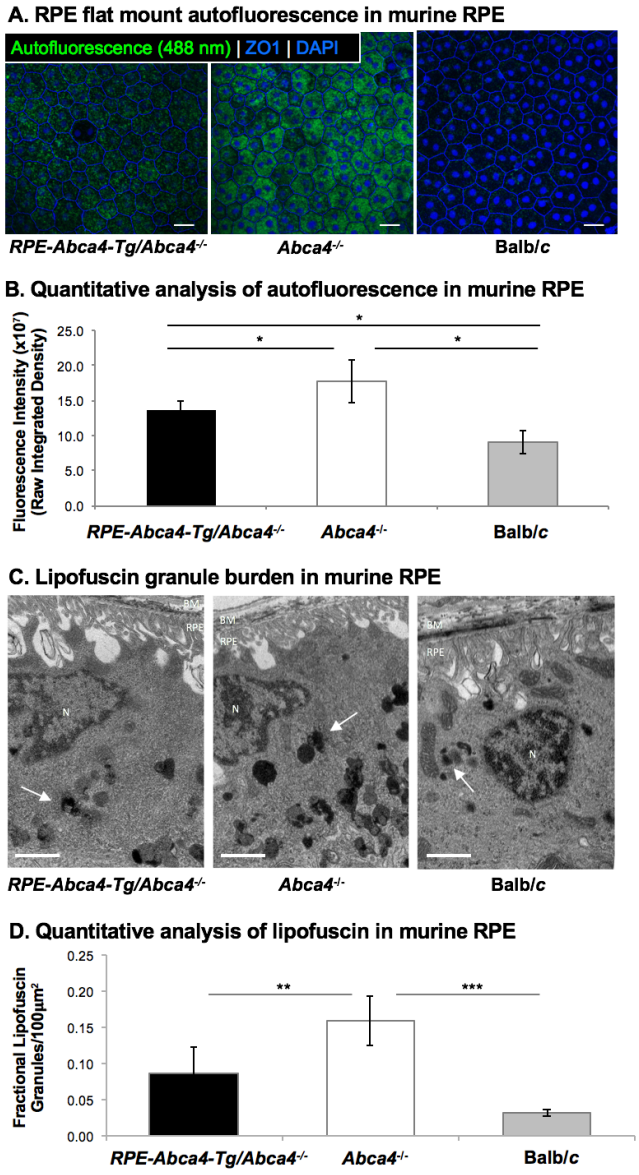

Figure 2.5. Reduced RPE flat mount autofluorescence and RPE lipofuscin burden in *RPE-Abca4-Tg/Abca4*$^{-/-}$ mice compared to *Abca4*$^{-/-}$ mice. (A) Representative confocal images of 6-month-old albino RPE-choroid-sclera flat mounts captured using a 488 nm excitation laser (and 500-545 emission filter) at 60x objective show varying levels of autofluorescence (green). RPE cell borders highlighted by anti-Zo-1 staining (blue); nuclei stained with DAPI (blue); scale bar = 20 μm. **(B)** Fluorescence intensity of the green channel was quantified by automated measure of raw integrated density units (x10^7) using ImageJ. Data presented as mean ± S.D. (n=3 mice per group); *p<0.001; *RPE-Abca4-Tg/Abca4*$^{-/-}$ vs. *Abca4*$^{-/-}$, p=0.0006; *Abca4*$^{-/-}$ vs. Balb/*c*, p<0.0001; *RPE-Abca4-Tg/Abca4*$^{-/-}$ vs. Balb/*c*, p<0.0001). **(C)** Representative electron microscopic images of RPE from 1-year-old albino mice showing polymorphic lipofuscin granules of mixed moderate- and high-electron density (white arrows) within RPE cytoplasm; BM = Bruch's membrane; RPE = retinal pigment epithelium; N = nucleus; Scale bar = 2 μm. **(D)** Fractional lipofuscin granules per 100 μm^2 cell area were measured and averaged from ten adjacent EM images per eye. Data presented as mean ± S.D. (n=5-9 mice per group); **p=0.0186; ***p=0.0013.

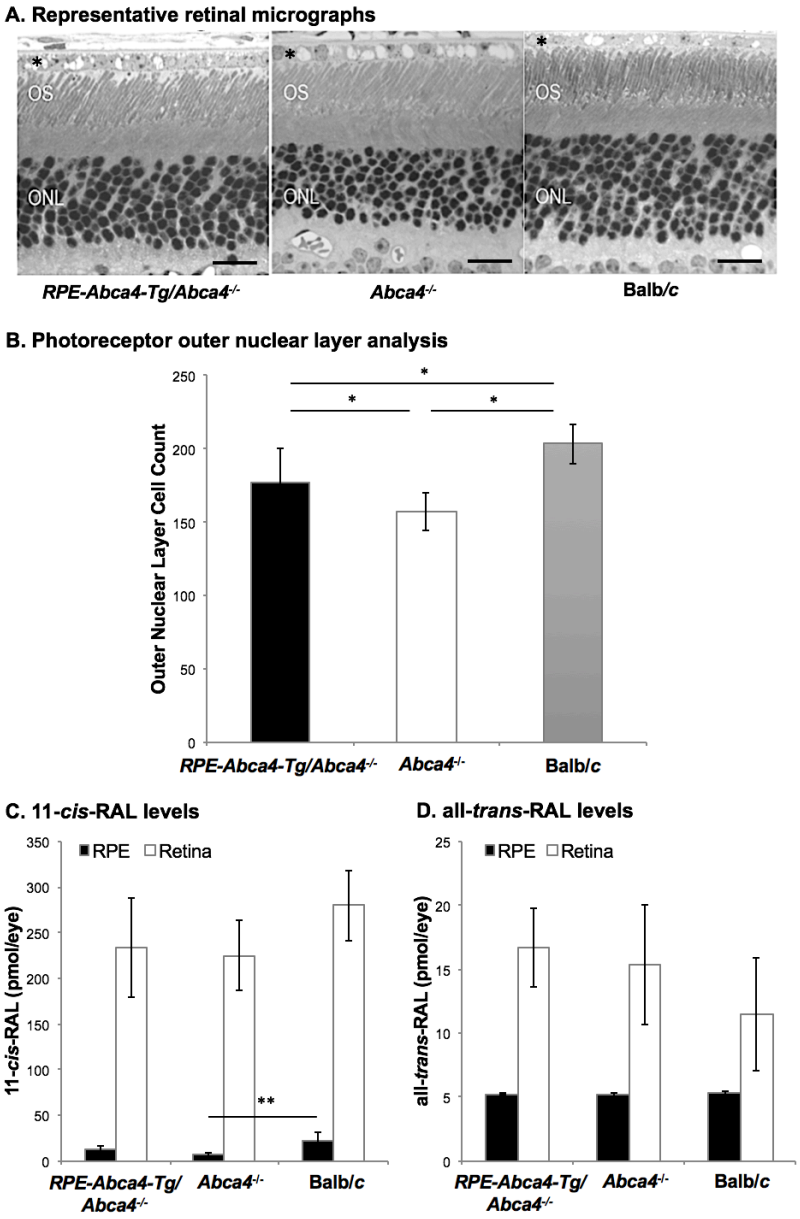

Figure 2.6. Photoreceptor preservation in *RPE-Abca4-Tg/Abca4*$^{-/-}$ mice compared to *Abca4*$^{-/-}$ mice. (A) Representative 1 µm retinal sections from 1-year-old albino mice taken with a light microscope at 63x objective; asterisk (*) denotes RPE layer; OS = outer segments; ONL = outer nuclear layer; scale bar = 20 µm. **(B)** Total number of photoreceptor nuclei were counted per 100 µm^2 cell area. Data presented as mean ± S.D. (n=5-9 mice per group); *p<0.05; *RPE-Abca4-Tg/Abca4*$^{-/-}$ vs. *Abca4*$^{-/-}$, p=0.0061; *Abca4*$^{-/-}$ vs. Balb/*c*, p<0.0001; *RPE-Abca4-Tg/Abca4*$^{-/-}$ vs. Balb/*c*, p=0.0319. In 3-month-old albino mice, 11-*cis*-RAL **(C)** and all-*trans*-RAL **(D)** levels are unchanged in both the RPE and retina of *RPE-Abca4-Tg/Abca4*$^{-/-}$ mice compared to *Abca4*$^{-/-}$ mice and Balb/c mice, although there is a significant difference in 11-*cis*-RAL levels in the RPE between *Abca4*$^{-/-}$ and Balb/*c* mice; **p=0.022. Data presented as mean ± S.D. (n=5 mice per group).

A. Scotopic *a*-wave ERG Intensity Response at 12 months

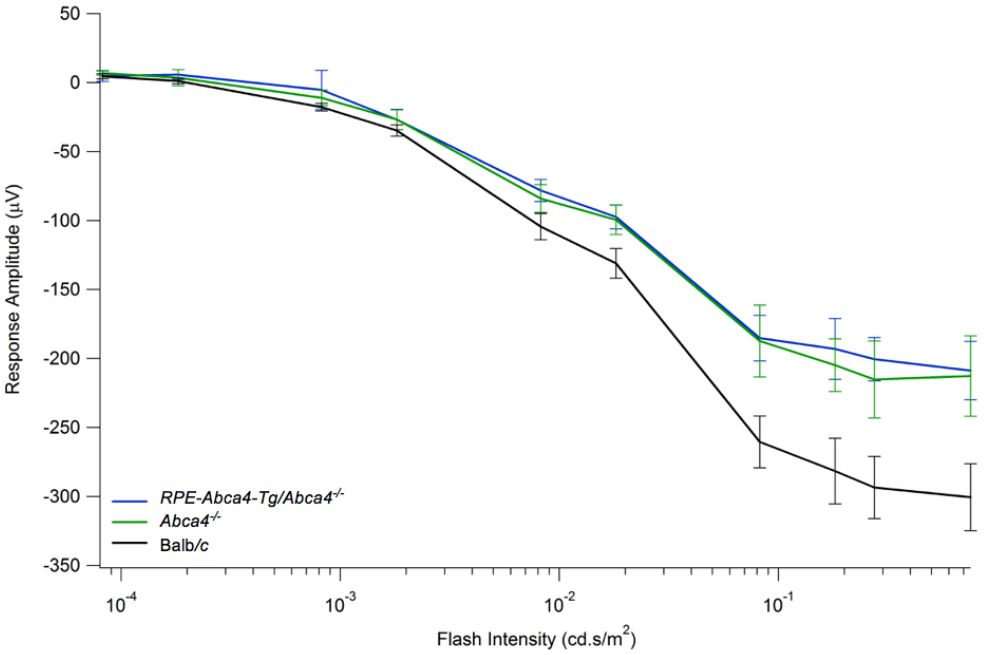

B. Scotopic *b*-wave ERG Intensity Response at 12 months

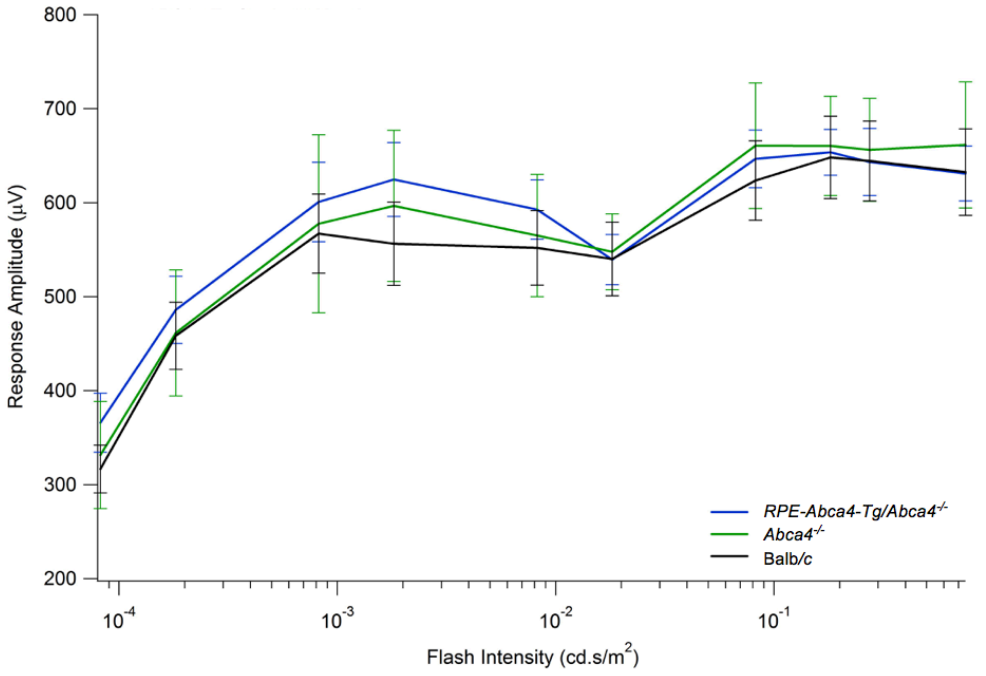

Figure 2.7. ERG recordings in one-year-old mice. Response amplitudes from scotopic *a*-wave **(A)** and *b*-wave **(B)** recordings were measured at varying flash intensities in overnight dark-adapted albino mice at one year of age. Differences in scotopic *a*-wave intensity responses are seen between Balb/*c* (black) vs. *Abca4*$^{-/-}$ (green) and Balb/*c* (black) vs. *RPE-Abca4-Tg*/*Abca4*$^{-/-}$ (blue) mice. No differences in scotopic *b*-wave intensity responses are seen between any of the groups. Data presented as mean ± S.D. (n=4-8 mice per group).

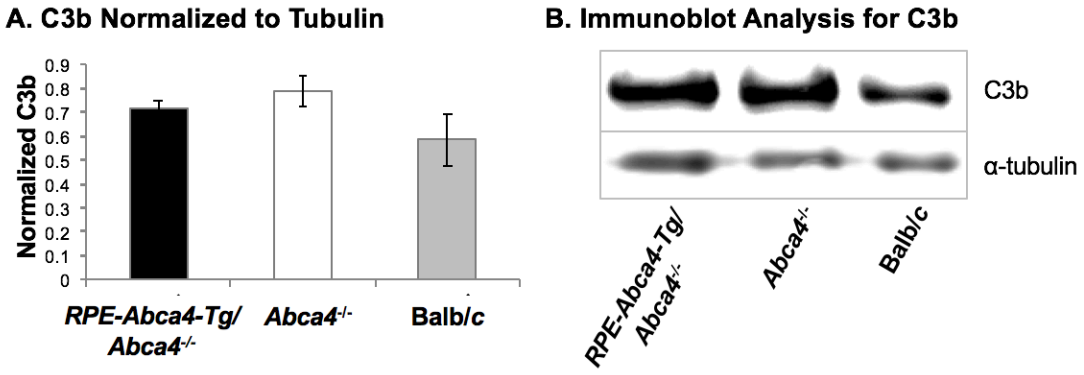

Figure 2.8. Reduced complement activation in the RPE of *RPE-Abca4-Tg/Abca4*$^{-/-}$ mice compared to *Abca4*$^{-/-}$ mice. (A) Quantitation of C3b protein levels, normalized to normalized to α-tubulin, in 6-month-old albino mice. **(B)** Representative immunoblots for C3b and α-tubulin from 25 µg of RPE protein homogenate.

Chapter 3: The role of RPE complement dysregulation in the *Abca4*$^{-/-}$ mouse model of recessive Stargardt disease (STGD1)

i. Introduction

Complement dysregulation in STGD1

The pathological hallmark of STGD1 is deposition of autofluorescent lipofuscin in the RPE[51,75]. Although lipofuscin deposition precedes retinal degeneration in STGD1 patients, the exact mechanism of how RPE lipofuscin accumulation disrupts overall RPE performance and leads to loss of macular photoreceptors is poorly understood[38]. The major lipofuscin component in the RPE of *Abca4*$^{-/-}$ mice and STGD1 patients, A2E[12,33], exerts cytotoxic effects through a variety of different and possibly linked mechanisms such as oxidative stress, lysosomal dysfunction, disrupted autophagy, and interference with cholesterol metabolism[52-64]. Furthermore, bisretinoids and their oxidation products have been shown to directly activate complement in RPE cell culture[57,76].

Complement dysregulation is implicated in the pathogenesis STGD1, as increased inflammatory markers and complement reactivity have been observed in *Abca4*$^{-/-}$ mice[52]. Furthermore, mutations in complement regulatory proteins have been identified as strong susceptibility factors in patients with age-related macular degeneration (AMD), which shares several phenotypic features with STGD1 including the presence of lipofuscin-laden RPE drusen[77-84]. A proposed link between bisretinoid accumulation and complement-mediated RPE injury includes the loss of cellular protective responses against complement due to A2E-induced perturbed cholesterol metabolism and increased oxidative stress[70]. Degeneration of photoreceptors in these animals has been attributed to degraded RPE function due to chronic bisretinoid-mediated complement dysregulation[52,85].

Modulation of complement regulatory proteins as a potential treatment for STGD1

The RPE fulfills several photoreceptor support functions including phagocytosis of distal outer segments (OS) and processing of visual retinoids[24,86-88]. Additionally, the RPE plays a major role in controlling the ocular immune response through expression of various complement negative regulatory proteins (CRP's)[89]. For these reasons, photoreceptors are critically dependent upon a healthy RPE for continued viability. Chapter 3 of this dissertation provides direct evidence that inappropriate complement activation plays a role in the pathogenesis of STGD1, especially given the rescue of *Abca4*$^{-/-}$ pathology seen with complement regulation. Specifically, this chapter describes the biochemical and morphologic protection achieved by normalizing complement activity with subretinal injection of recombinant adeno-associated virus containing the gene for the CRP, complement receptor 1-like protein y (CRRY).

ii. Viral gene therapy-mediated complement modulation in the RPE rescues photoreceptor degeneration in the *Abca4*$^{-/-}$ mouse model of STGD1

Subretinal AAV-CRRY delivery increases CRRY expression in the RPE

The murine CRRY gene was subcloned with a c-Myc (Myc) tag into the pAAV8-CAG-MCS plasmid vector to generate the CRRY-Myc construct (Fig. 3.1A), which was packaged into an AAV type 2 vector genome pseudo-serotyped with the RPE-tropic AAV type 8 capsid (AAV2/8). The recombinant adeno-associated virus containing the gene for CRRY (AAV-CRRY) was then subretinally injected under direct visualization and confirmed by fundus imaging and OCT in 4-week-old mice. Either 13,000 MOI of AAV-CRRY or control AAV2/8 (AAV-null) virus in 0.5 μl injection volume was delivered. The CRRY construct designed with a Myc tag allowed us to distinguish the AAV-expressed protein from endogenous CRRY. We confirmed expression of Myc-tagged CRRY protein in RPE homogenates of *Abca4*$^{-/-}$ mice by immunoblotting, five weeks

after subretinal injection. In AAV-CRRY RPE homogenates, the protein was detected by both CRRY and Myc antibodies, whereas RPE homogenates from uninjected and null-injected (AAV-GFP) *Abca4-/-* mice only exhibited reactivity with the CRRY antibody (Fig. 3.1B). However, Myc-immunoreactivity was undetectable in the neural retina homogenates suggesting RPE specificity. CRRY mRNA expression was measured by qRT-PCR using cDNA from mouse RPE as the template. By one year post-injection, the CRRY mRNA was four-fold more abundant in AAV-CRRY injected versus AAV-Null injected *Abca4-/-* mice (Fig. 3.2A**)**. Consistently, levels of recombinant CRRY were higher in RPE homogenates from AAV-CRRY-injected versus AAV-Null-injected mice by immunoblotting, using antibodies against CRRY and Myc (Fig. 3.2B). These results indicate stable long-term expression of AAV-CRRY. Expression of other CRP mRNAs was not significantly altered in the RPE of AAV-CRRY-injected *Abca4-/-* mice (Fig. 3.2A).

CRRY overexpression correlates with decreased accumulation of complement C3 and its breakdown fragments in the RPE

Complement factor C3 is cleaved to generate the C3bBb convertase, C3b and its breakdown fragment (iC3b) upon initiation of the complement cascade. To determine whether overexpression of CRRY resulted in decreased C3 convertase, we evaluated C3/C3b levels in the eyes of injected animals by immunohistochemistry and quantitative immunoblotting. C3/C3b immunofluorescence was reduced in RPE sections from AAV-CRRY- vs. AAV-Null-injected mice (Fig. 3.3A). In these animals, CRRY overexpression was confined to the RPE by Myc immunofluorescence (Fig. 3.3A). To confirm this finding, we measured C3 in RPE homogenates by quantitative immunoblotting. At one year of age, C3/C3b levels were two-fold lower in AAV-CRRY- vs. AAV-Null-injected mice (Fig. 3.3B). These results suggest that overexpression of CRRY reduced complement activation on the RPE, as intended.

RPE autofluorescence is decreased in the AAV-CRRY-injected Abca4$^{-/-}$ mice

Accumulation of autofluorescent bisretinoids in the RPE is a hallmark of STGD1[33]. It was previously shown that C3 breakdown fragments get internalized in the RPE cells of *Abca4*$^{-/-}$ mice and co-localize with endogenous autofluorescence[52]. We investigated the distribution of CRRY by immunofluorescence and the distribution of autofluorescent bisretinoids in RPE flat mounts from 6-month-old *Abca4*$^{-/-}$ mice.

AAV-CRRY-injected *Abca4*$^{-/-}$ mice exhibited significantly lower autofluorescence in the RPE compared to AAV-Null-injected *Abca4*$^{-/-}$ mice (Fig. 3.4). Age-matched wild-type (Balb/c) controls also exhibited lower autofluorescence in the RPE compared to AAV-Null-injected *Abca4*$^{-/-}$ mice, as anticipated (Fig. 3.4). Only the AAV-CRRY-injected mice showed significant Myc immunofluorescence in the RPE (Fig. 3.4). Subretinal injection of the virus in the superior-temporal region only covered approximately one-third of the retina; the flat mounts in (Fig. 3.4) are from this treated area.

As expected, RPE from an inferior-nasal region remote from the superior-temporal site of injection exhibited minimal Myc immunofluorescence (Fig. 3.5, away from injection site). Additionally, RPE autofluorescence was higher in this non-rescued region (Fig. 3.5), suggesting a correlation between CRRY overexpression and reduced bisretinoid accumulation in the RPE of *Abca4*$^{-/-}$ mice.

Bisretinoid levels are reduced in AAV-CRRY-injected Abca4$^{-/-}$ mice

We quantified bisretinoids fluorophores by HPLC in wild type and *Abca4*$^{-/-}$ RPE at 11-12 months post-injection. Both A2PE-H_2 and A2E were ~2.5-fold reduced in *Abca4*$^{-/-}$ mice that received the AAV-CRRY vs. those that received the AAV-Null virus (Fig. 3.6). Still lower levels of bisretinoids were present in uninjected, age-matched wild type mice (Fig. 3.6).

CRRY-overexpression did not affect oxidative stress or autophagy in Abca4$^{-/-}$ RPE

Bisretinoid accumulation in the RPE is partly responsible for inducing cellular oxidative stress and compromised autophagy[52,71]. We measured mRNA and protein expression of cytoplasmic superoxide dismutase 1 (SOD-1) along with mitochondrial superoxide dismutase 2 (SOD-2), in the eyes of 7-month-old AAV-CRRY- and AAV-Null-injected mice by qRT-PCR and immunoblotting (Fig. 3.7). SOD-1 and SOD-2 mRNA and protein levels were present at similar levels in the RPE cells of AAV-CRRY- and AAV-Null-injected mice (Fig. 3.7). We also measured the lipidated form of microtubule-associated protein light chain 3B (LC3) in the RPE of wild type and *Abca4*$^{-/-}$ mice, six months following subretinal injection of AAV-CRRY or AAV-Null virus. We observed a significant decrease in LC3 levels in RPE homogenates from *Abca4*$^{-/-}$ vs. age-matched wild type mice (Fig. 3.8). However, LC3 immunoreactivity was not influenced by CRRY over-expression in either wild type or *Abca4*$^{-/-}$ RPE (Fig. 3.8). Thus, oxidative stress and impaired autophagy may not be improved by increasing CRRY expression.

Lipofuscin deposition in the RPE cells is decreased after AAV-CRRY injection

Accumulation of lipofuscin granules in the RPE occurs with normal aging and is greatly accelerated in *Abca4*$^{-/-}$ mice[12,90]. Electron microscopic analysis of retinal sections from AAV-CRRY-injected *Abca4*$^{-/-}$ eyes showed significantly reduced pigment granules in the RPE cells compared to AAV-Null-injected *Abca4*$^{-/-}$ eyes (Fig. 3.9). To quantify these lipofuscin pigments, we measured the RPE cell area occupied with pigment granules divided by the total cytoplasmic area. The fractional area of lipofuscin granules in the RPE of AAV-CRRY-injected *Abca4*$^{-/-}$ eyes was ~30% lower than that of AAV-Null-injected *Abca4*$^{-/-}$ eyes (Fig. 3.9). However, both AAV-CRRY- and AAV-Null-injected *Abca4*$^{-/-}$ eyes show 2.5-fold and 1.8-fold respectively higher lipofuscin deposition in comparison to uninjected wild type eyes (Fig. 3.9).

Overexpression of CRRY in the RPE protects Abca4$^{-/-}$ photoreceptors from degeneration

Albino *Abca4*$^{-/-}$ mice exhibit slow degeneration of photoreceptors[91]. In order to test whether overexpression of CRRY in the RPE of *Abca4*$^{-/-}$ mice had a protective effect, we performed light microscopy on fixed retinal sections from regions overlying the site of virus injection from 1-year-old mice. AAV-CRRY-injected *Abca4*$^{-/-}$ mice exhibited significantly more photoreceptor nuclei in the outer nuclear layer (ONL) compared to AAV-Null-injected *Abca4*$^{-/-}$ mice (Fig. 3.10). In the rescued area, the number of ONL nuclei were similar in AAV-CRRY-injected *Abca4*$^{-/-}$ and wild type mice (Fig. 3.10).

These results suggest nearly complete protection from photoreceptor degeneration in the injected region (superior-temporal). To confirm these findings, we determined levels of 11-*cis*-retinaldehyde (11-*cis*-RAL) chromophore in dark adapted mice, which correlates with the number of rhodopsin molecules. At ~11 months post-injection, AAV-CRRY-injected *Abca4*$^{-/-}$ eyes contained 25% more 11-*cis*-RAL than AAV-Null-injected *Abca4*$^{-/-}$ eyes (Fig. 3.11). Still higher levels of 11-*cis*-RAL were present in age-matched wild type control mice (Fig. 3.11). The less dramatic rescue of photoreceptor degeneration by 11-*cis*-RAL levels likely reflects the averaging of protected and non-protected areas in the AAV-CRRY-injected mice.

iii. Materials and methods

Animals: Albino *Abca4*$^{-/-}$ and Balb*/c* mice were housed in 12-hour light/12-hour dark conditions and fed *ad libitum*. Mice were on the homozygous *Rpe65* Leu450 variant and free of the *rd8* mutation in *Crb1*. All experiments were performed in accordance with the Association for Research in Vision and Ophthalmology (ARVO) statement and University of California Institutional Animal Care and Use Committee (IACUC) guidelines for animal care and approved research protocols.

Generation of adeno-associated viral vector expressing CRRY: Murine CRRY gene[92] was amplified by polymerization chain reaction (PCR) from cDNA clone (Origene NM_013499). A carboxy terminal c-Myc tag was added using oligonucleotides (Forward: 5' CACACACGCTAGCCCTCTTAAAAGATCCAAAAAATGAGACTTCTAGC 3' and Reverse: 5' TGTGTGCTCGAGTTACAGATCCTCTTCTGAGATGAGTTTTTGTTCGG AGACTTCTTGAGTGAGTGAATTCCGTG 3') and subcloned into pAAV8-CAG-MCS (Vector Biolabs, Malvern, PA) within restriction site XhoI to NheI to generate pAAV8-CAG-CRRY-Myc (CRRY-Myc, Fig. 3.1A). The construct was verified with restriction digests and by sequencing analysis. The CRRY-Myc construct (AAV-CRRY) was packaged in an AAV2 vector genome pseudo-serotyped with the AAV type 8 capsid (AAV2/8) by the Penn Vector Core (Philadelphia, PA)[93]. Control vector such as AAV2/8 null (AAV-Null) and a vector expressing green-fluorescence protein (AAV-GFP) were obtained from Signagen laboratories (Rockville, MD).

Subretinal injections: Mouse eyes were dilated with 2.5% phenylephrine (Hub Pharmaceuticals, Rancho Cucamonga, CA) and 0.5% tropicamide (Akorn Pharmaceuticals, Lake Forest, IL). Mice were anesthetized with 100 mg/kg of ketamine (Phoenix Pharmaceuticals, Burlingame, CA) and 8 mg/kg of xylazine (Lloyd Laboratories, Shenandoah, IA). Prior to injection, the AAV-CRRY, -GFP, and -Null vector stock solutions were diluted from a $2x10^{12}$ - $2x10^{13}$ GC/ml to deliver about 13,000 multiplicities of infection (MOI) in 0.5 µl volume. A multi-purpose 2.7 mm telescoping modified-endoscope (Karl Storz, Tuttlingen, Germany) was used to perform the subretinal injections in the superior-temporal quadrant under direct visual control. The endoscope tip was illuminated via a fiber optic cable connected to a xenon light source and connected to a high definition camera and Image 1 Hub monitor (Karl Storz). A superior-temporal scleral incision was made with a 33g needle followed by insertion of a blunt tip 33g

needle on a Hamilton syringe. Successful injections were identified by optical coherence tomography (OCT, Bioptigen, Morrisville, NC) and fundus imaging (Karl Storz) immediately following injection and at different time points thereafter. The mice were kept on a 37°C heating pad during the subretinal injection, recovery after the anesthesia, and follow-up fundus examination. Eyes presenting with evidence of retinal damage or hemorrhage by fundus visualization or OCT were excluded from further analysis.

Quantitative real-time RT-PCR: Total RNA was extracted from mouse RPE homogenate using an Absolutely RNA Miniprep kit (Stratagene, La Jolla, CA) with DNAase treatment and reverse-transcribed to cDNA using SuperScript III (Invitrogen) according to the manufacturer's protocol. Quantitative real-time PCR (qRT-PCR) was performed with SYBR Green (Invitrogen) and mouse gene specific primer sets for CRRY, DAF1, DAF2, CD59a, CD59b, CFH, SOD-1, and SOD-2 following a previously reported protocol [52]. RNA expression was normalized to 18S rRNA Ct-values for each sample, and relative mRNA levels were presented as means with standard deviation (S.D.; n=5 eyes for each group).

Immunoblotting: RPE/eyecup vs. neural retina tissue from each animal was homogenized in 1xPBS with Halt protease inhibitor cocktail (Life Technologies, Carlsbad, CA). Protein samples were treated with Benzonase nuclease (Sigma-Aldrich) at room temperature for one hour and re-homogenized with 1% SDS. Cellular debris was removed using centrifugation and protein concentration was determined using Micro BCA assay (Thermo Scientific, Waltham, MA). Proteins were then separated on 4-12% SDS-PAGE gels (Novex, Invitrogen, Carlsbad, CA) as previously described [52]. Membranes were blocked with Odyssey blocking buffer (LI-COR Biosciences, Lincoln, NE) followed by incubation at room temperature and probed with the following antibodies: Myc (c-myc, PA1-22826; Thermo Scientific, Waltham, MA); α-tubulin

(T9026), LC3 (L7543) from Sigma Aldrich (St. Louis, MO); β-actin (A00702; Genscript, Piscataway, NJ); C3/C3b/iC3b (HM1065; Hycult Biotech, Plymouth Meeting, PA); CRRY (sc-30214), SOD-1 (sc-11407), SOD-2 (sc-30080) from Santa Cruz Biotechnology (Santa Cruz, CA). The predominant isoforms of recombinant CRRY detected by CRRY antibody were 53 kDa and 65 kDa; Myc immunostaining consistently confirmed recombinant CRRY expression. Western blotting was performed using cognate IR-dye labeled secondary antibodies and detected with an Odyssey CLx infrared imaging system (LI-COR).

Immunocytochemistry: Prior to enucleation, all eyes were marked by cauterization on the superior pole. The eyes were immersion fixed in 4% paraformaldehyde for two hours on ice for RPE-choroid-sclera flat mounts or overnight at 4°C for frozen section. For frozen sections, each eye was embedded in cryo-OCT (Tissue-Tek) and cut into 10 µm sections for and C3/C3b and Myc immunohistochemistry as previously described[52]. For flat mounts, eyecups were dissected into eight leaflets, permeabilized with 1% Triton-X 100, and blocked with 1% BSA/5% NGS in 0.1M NaPO4 buffer (pH 7.0). RPE-choroid-sclera flat mounts were incubated overnight at 4°C with anti-rabbit ZO-1 (61-7300; Thermo Scientific, Waltham, MA) and anti-mouse c-myc (PA1-22826) and then stained with goat anti-rabbit Alexa Fluor 647 conjugate and anti-mouse Alexa Fluor 568 conjugate secondary antibodies for one hour at room temperature. The RPE flat mounts (with apical RPE facing up) and retinal sections were mounted in Prolong Gold anti-fade reagent containing DAPI nuclear staining (Life Technologies, Carlsbad, CA) and imaged from the superior-temporal quadrant using a 60x oil-immersion lens with an Olympus Fluoview FV1000 confocal microscope. The RPE flat mounts were imaged at a single, 3-µm-thick Z-plane at the mid RPE level. RPE autofluorescence was evaluated using an excitation wavelength of 488 nm and emission filter of 515 to 565 nm.

Light and electron microscopy: Mice were euthanized under anesthesia and fixed by intra-cardiac perfusion with 2% formaldehyde and 2.5% glutaraldehyde in 0.1 M sodium phosphate buffer, pH 7.2. The nasal and temporal hemispheres of each eyecup were separated and fixed additionally in 1% osmium tetroxide dissolved with 0.1 M sodium phosphate then dehydrated in a graded series of alcohols. The temporal hemispheres were embedded in an tEpon-812 (Tousimis Research Corporation, Rockville, MD) / Araldite mix (Electron Microscopy Sciences, Hartfield, PA) for light microscopy. Sections of 1 μm thickness stained with Toluidine blue were imaged in the region of the injected quadrant (superior-temporal) at 63x objective using a CoolSNAP digital camera (Photometrics, Tucson, AZ) affixed to a Zeiss Axiophot microscope (Zeiss, Thornwood, NY). Total number of photoreceptor nuclei in three independent areas in the region of the injection site (superior-temporal quadrant) were counted and plotted in PrismGraph program. Data is presented as means with S.D. (AAV-Null-injected *Abca4*$^{-/-}$: n=6 eyes; AAV-CRRY-injected *Abca4*$^{-/-}$: n=11 eyes; uninjected Balb/*c*: n=4 eyes). The nasal hemispheres were cut into quadrants and embedded in Araldite 502 (Electron Microscope Sciences) for EM. Ultrathin sections were cut on a Leica Ultracut microtome, collected on 200 mesh copper grids, and double stained with uranium and lead salts. The ultrathin sections were imaged on a JEM 1200-EX (JEOL, Peabody, MA) electron microscope. At least ten images of 100 μm^2 area were acquired from the superior-nasal quadrant of each eye at 15,000x magnification. Using Soft-imaging software (Olympus Soft Imaging Solutions, EMSIS, GmbH, Münster, Germany), fractional lipofuscin granules were measured by obtaining the area in μm^2 occupied by lipofuscin over the area in μm^2 occupied by cytoplasm. Each animal's fractional lipofuscin granule measurement corresponded to an average of at least ten adjacent EM images from one eye (n=5-9 animals per group).

Quantification of retinoids and bisretinoids: Retinoids and bisretinoids levels in the mouse whole eye were determined using published methods[52,94]. Mice were dark-adapted overnight and all tissue manipulations were performed under dim red light (Kodak Wratten 1A filter). Each whole eye was homogenized in 1x PBS, mixed with chloroform/methanol (2:1, v/v), and extracted with chloroform for bisretinoids analysis. For 11-*cis*-retinaldehyde (11-*cis*-RAL) quantification, whole eye homogenization was done in the presence of hydroxylamine and extracted in hexane. The organic phase was dried under argon stream and resuspended in 100 μl of isopropanol and 100 μl of hexane respectively. Absorption units corresponding to the A2E peak at 435 nm were converted to picomoles (pmol) using a calibration curve with an authentic A2E standard and the published molar extinction coefficient for A2E[74]. Eluted retinal oxime peaks were identified by spectra and elution time, and absorption units were converted to pmol using a calibration curve based on authentic standards and published molar extinction coefficients[95].

Statistical analysis: The results were presented as means with S.D. of a minimum of four to six animals per group unless otherwise specified. Two-group comparisons were performed using the Student's *t*-test in Microsoft Excel, whereas multiple group comparisons were performed using one-way ANOVA with Tukey's post-hoc analysis in JMP Pro v12 (SAS Institute, Cary, NC).

iv. Figures

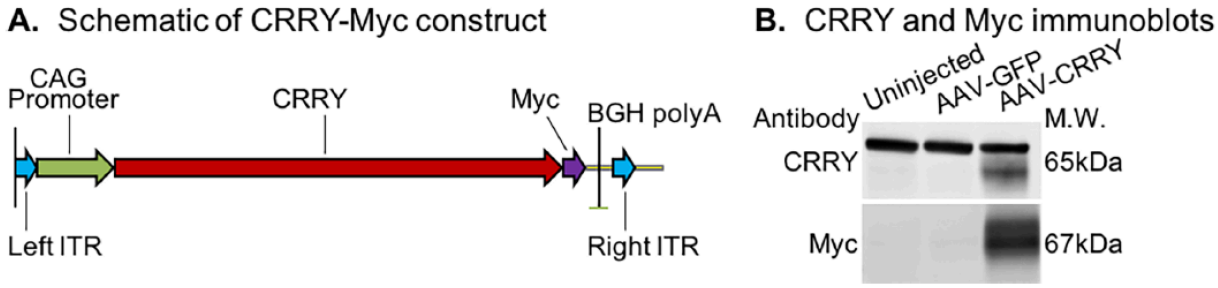

Figure 3.1. AAV-CRRY construct to express a Myc-tagged CRRY protein delivered by subretinal injection. **(A)** Schematic of CRRY-Myc construct delivered by subretinal injection. **(B)** Representative immunoblot of CRRY and Myc using RPE homogenate (10 μg protein per lane) from 2-month-old mice at five weeks post-subretinal injection of 0.5 μl of AAV-CRRY construct. Note: Myc immunoreactivity is observed only in the mice injected with AAV-CRRY whereas CRRY antibody binding is present in all tested samples.

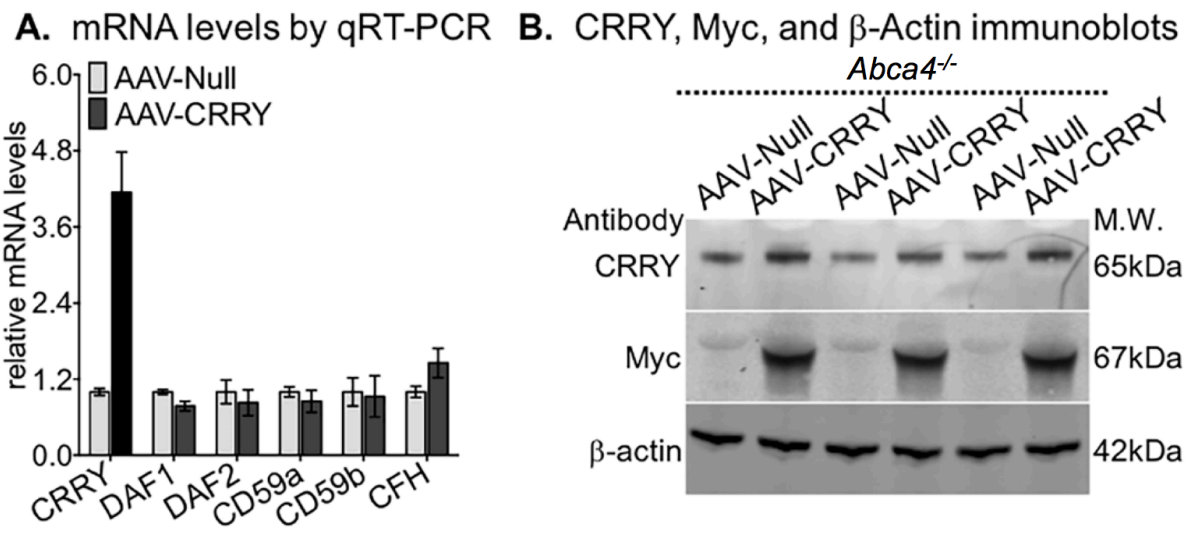

Figure 3.2. Increased expression of CRRY in the RPE cells by subretinal injection of AAV-CRRY. (A) Histogram showing relative CRRY, DAF1, DAF2, CD59a, CD59b, and CFH mRNA levels by qRT-PCR. Each mRNA level was normalized to 18S rRNA. **(B)** Representative immunoblot of CRRY, Myc, and β-actin using RPE homogenate (10 μg protein per lane). Protein and cDNA samples were obtained from 1-year old *Abca4*$^{-/-}$ mice injected with AAV-CRRY and -Null viruses. Data presented as mean ± S.D. (n=5 mice per group; each protein and cDNA sample was run in triplicate).

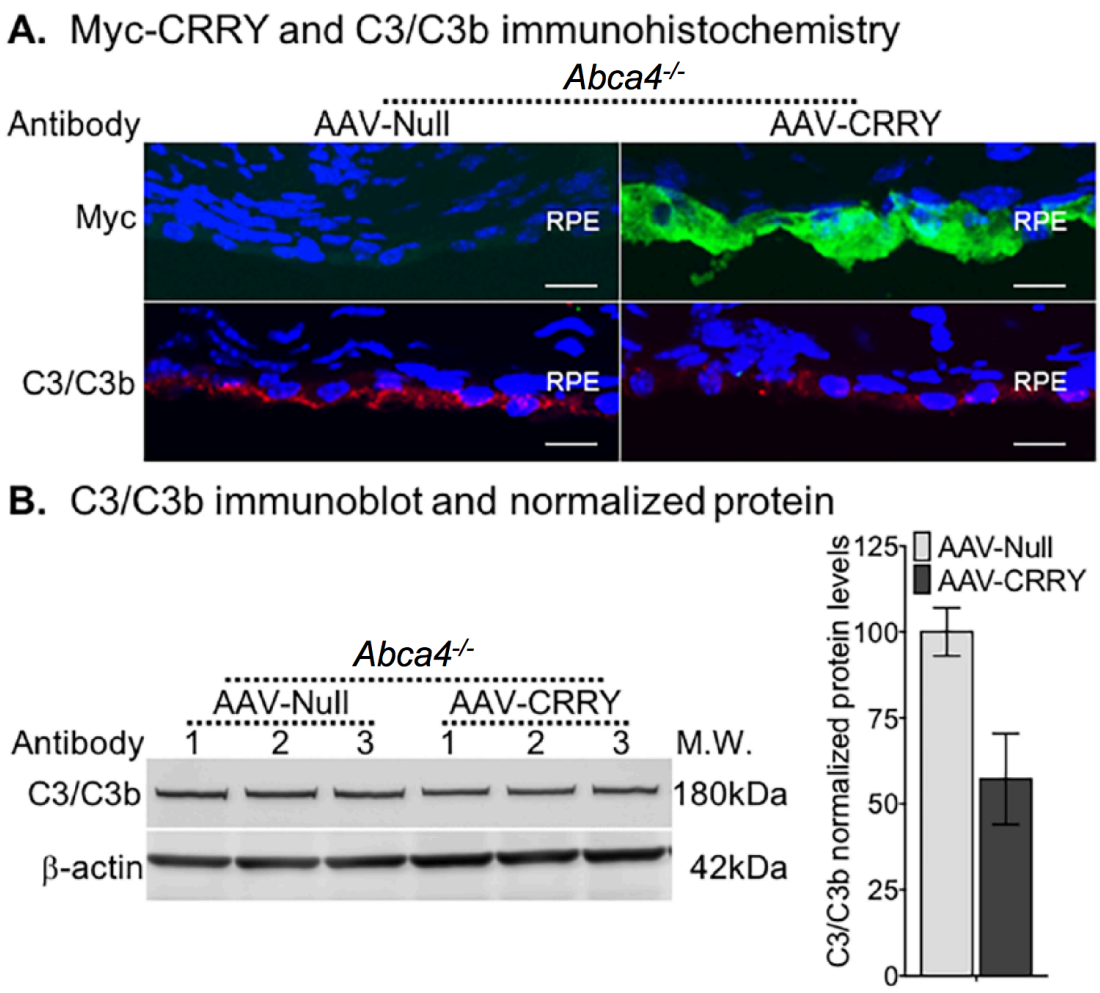

Figure 3.3. Reduced C3/C3b immunoreactivity in AAV-CRRY-treated *Abca4-/-* mice. (A) Representative confocal images of Myc (green), C3/C3b (red), and DAPI (blue) immunohistochemistry in 5-month-old *Abca4*$^{-/-}$ mice injected with AAV-CRRY and -Null viruses (n=3 mice per group). Scale bar = 10μm. **(B)** Representative immunoblot of Myc, C3/C3b, and β-actin using RPE homogenate (10 μg protein per lane). C3/C3b band intensity in RPE homogenate samples was normalized to β-actin. Note ~two-fold reduction in C3/C3b levels in the AAV-CRRY group. Data presented as mean ± S.D. (p<0.005; n=6 mice per group).

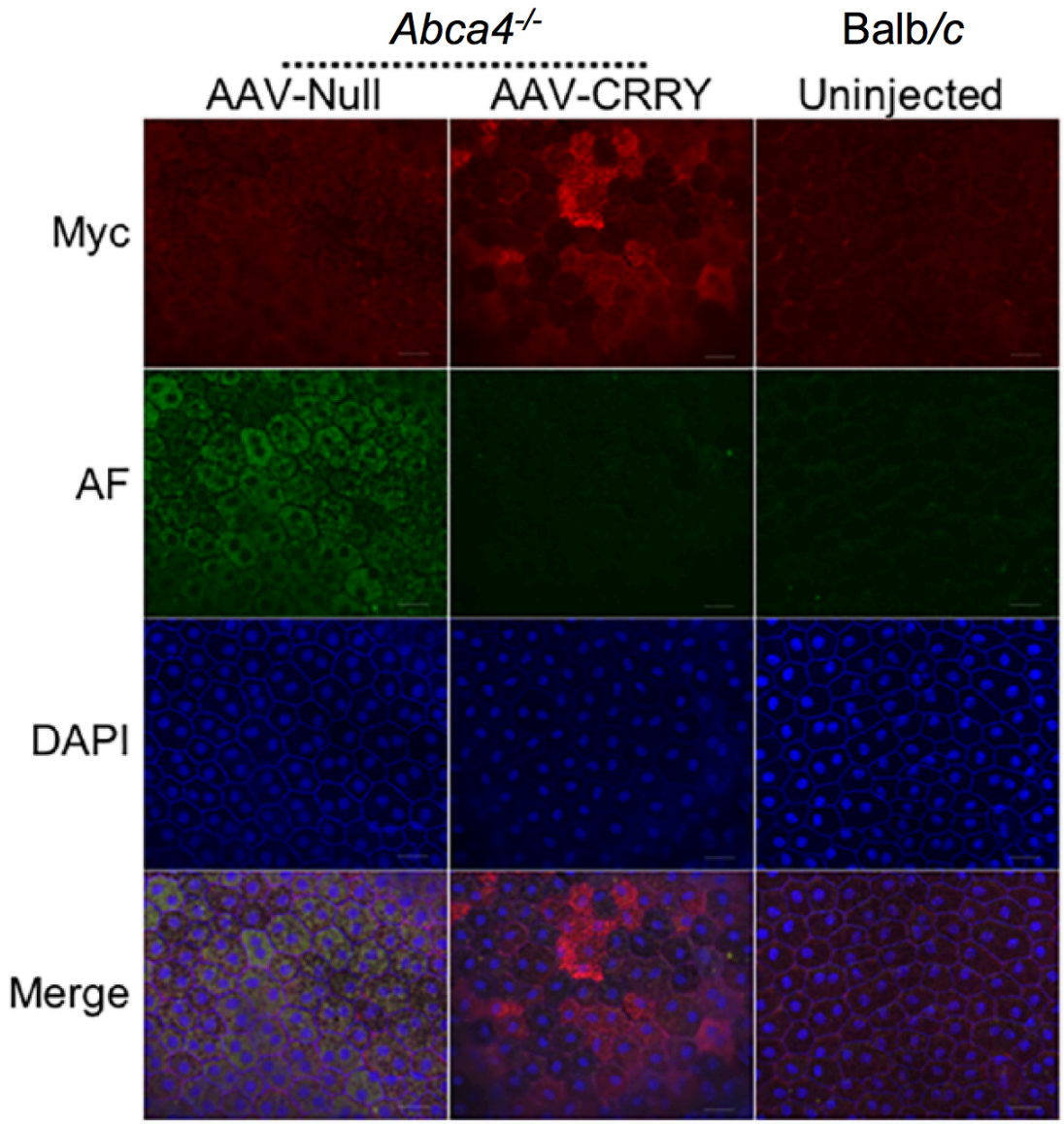

Figure 3.4. Decreased RPE autofluorescence in AAV-CRRY-injected *Abca4*$^{-/-}$ mice. Representative confocal images of Myc (red) and DAPI (blue) immunohistochemistry; autofluorescence (AF, green) acquired at 488nm in 6-month-old *Abca4*$^{-/-}$ mice injected with AAV-CRRY or -Null virus (left and middle columns) and age-matched, untreated Balb/*c* control mice (right column). (n=4 mice per group). Scale bar = 20 μm. Autofluorescence intensity inversely correlates with levels of Myc-CRRY expression in the *Abca4*$^{-/-}$ mice.

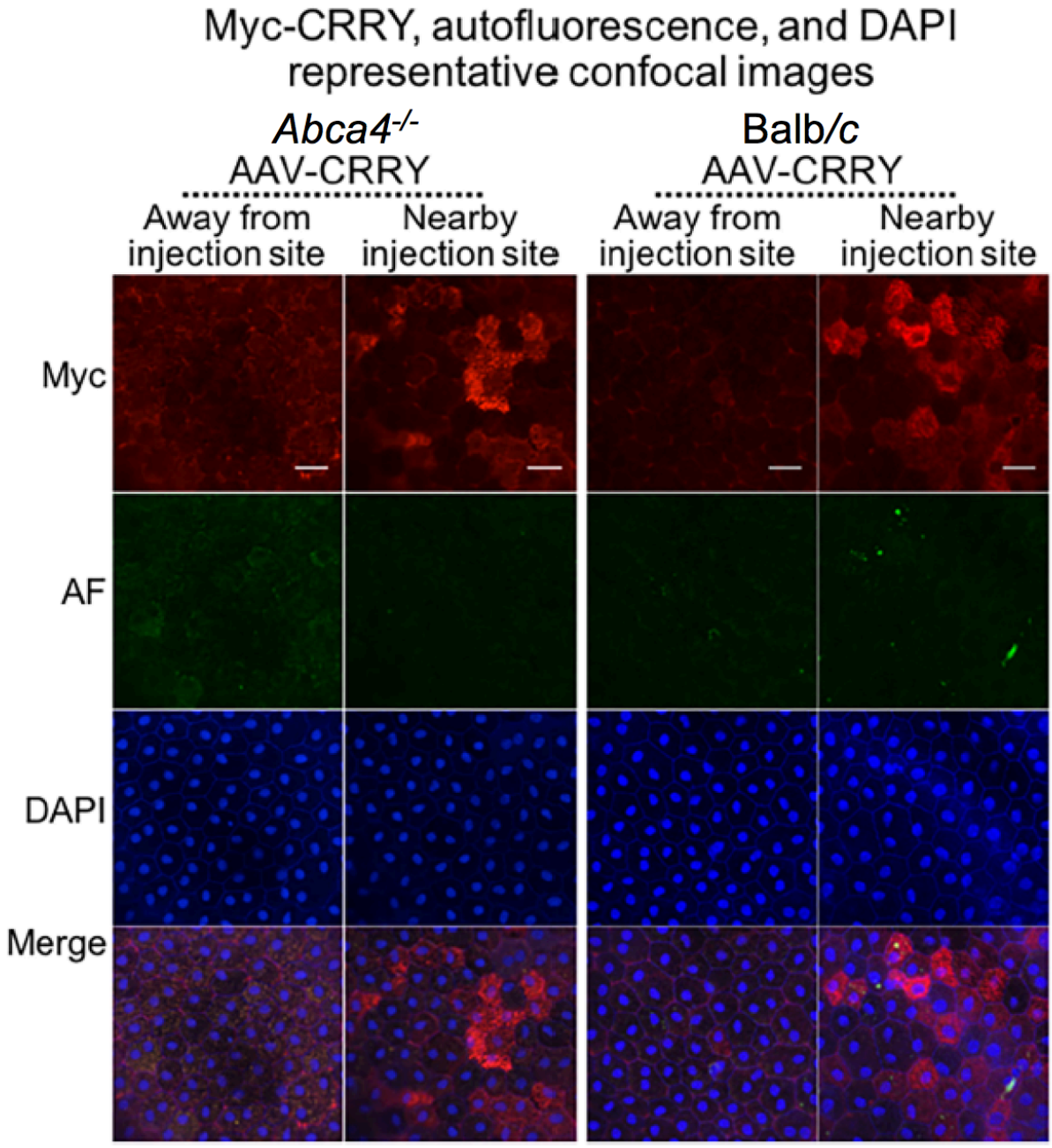

Figure 3.5. RPE autofluorescence pattern and CRRY-Myc staining in CRRY-injected *Abca4*$^{-/-}$ and Balb/*c* mice. Representative confocal images of Myc (red) and DAPI (blue) immunohistochemistry; autofluorescence (AF, green) acquired at 488nm of 7-month-old AAV-CRRY-injected *Abca4*$^{-/-}$ (left two columns) and Balb/*c* (right two columns) mice. Note increased Myc immunostaining of RPE cells in the area *nearby* the injection site corresponding with the superior-temporal quadrant (top row, second and fourth columns). In contrast, there is no Myc immunostaining of RPE cells in the area away from the injection site corresponding with the inferior-nasal quadrant. Autofluorescence (green) distribution is inversely related to Myc immunoreactivity for the *Abca4*$^{-/-}$ mice, whereas Balb/*c* mice show negligible RPE autofluorescence. Scale bar = 20 μm.

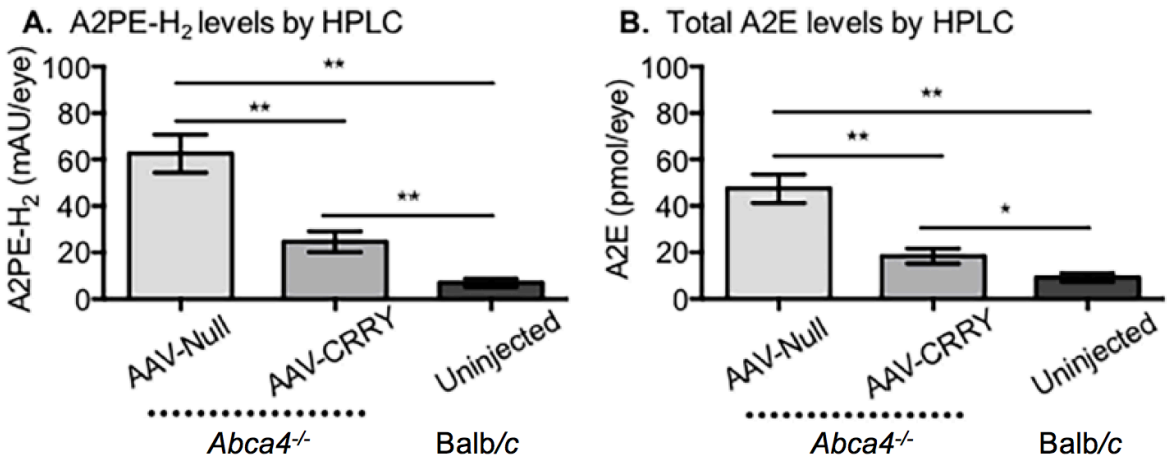

Figure 3.6. Reduced bisretinoid levels in AAV-CRRY-injected *Abca4*$^{-/-}$ mice. Bisretinoids were quantified by HPLC from RPE chloroform extracts of a single eyecup from 1-year-old mice. **(A)** A2PE-H_2 and **(B)** A2E are expressed as milliabsorbance units (mAU) and picomoles (pmol) per eye respectively. Data presented as mean ± S.D. (n=6-8 mice per group; *p<0.05, **p<0.005).

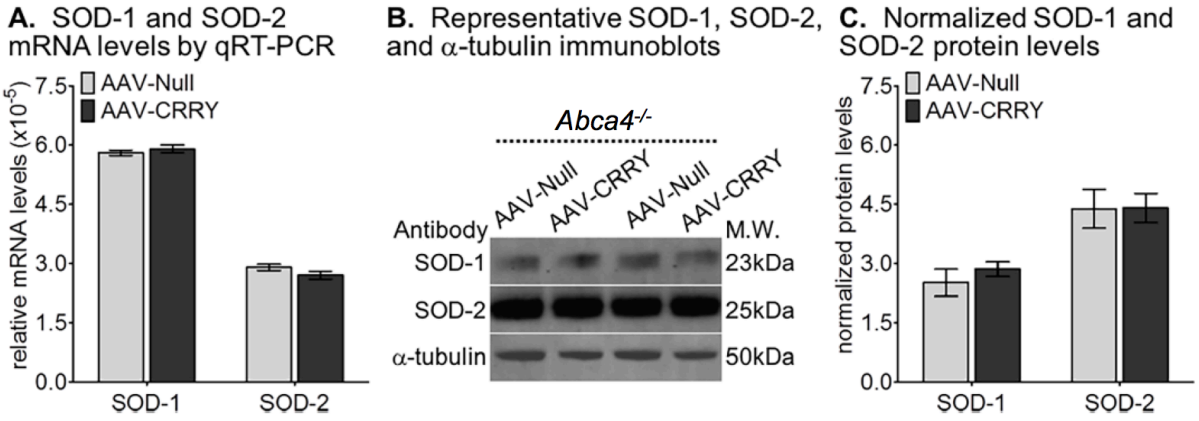

Figure 3.7. AAV-CRRY treatment does not change the oxidative stress level in *Abca4*$^{-/-}$ mice. (A) Histogram showing the relative SOD-1 and SOD-2 mRNA levels by qRT-PCR. Each mRNA level was normalized to 18S rRNA. **(B)** Representative immunoblots of SOD-1, SOD-2, and α-tubulin using RPE homogenate (10 μg protein per lane). **(C)** Histogram showing SOD-1 and SOD-2 normalized protein data in the RPE homogenate samples. Protein and cDNA samples were obtained from 7-month-old *Abca4*$^{-/-}$ mice injected with AAV-CRRY or -Null viruses. Data presented as mean ± S.D. (n=4 mice per group; each protein and cDNA sample was run in triplicate).

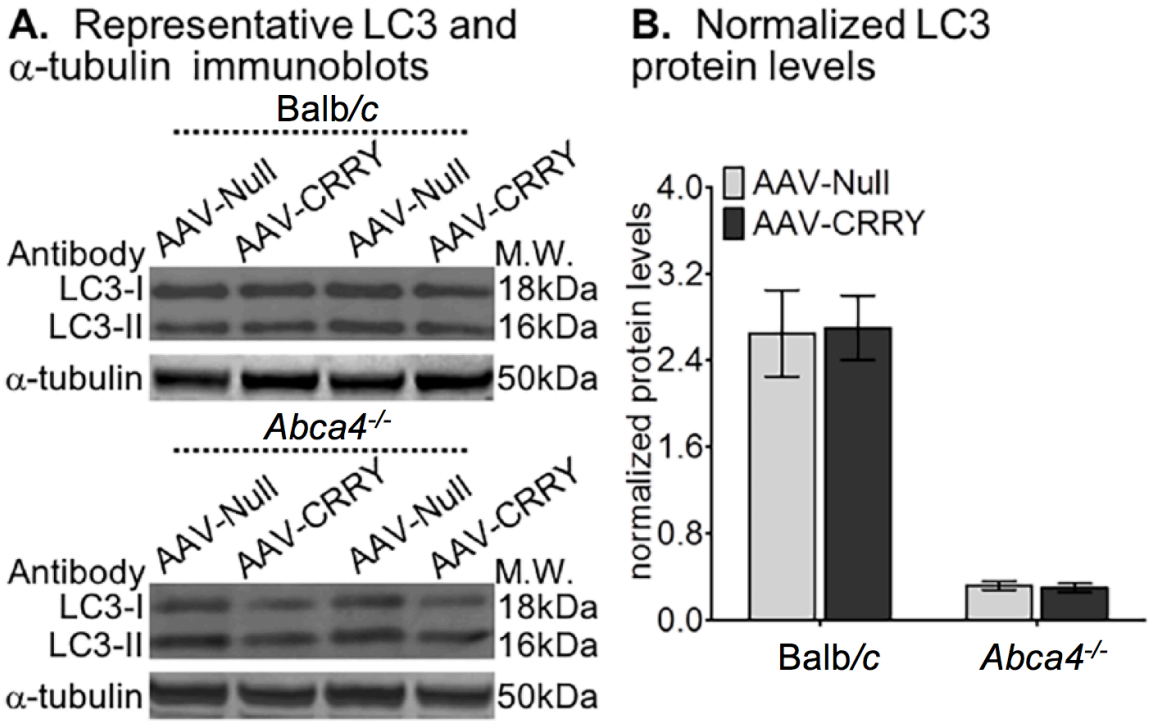

Figure 3.8. LC3 activity in the RPE of *Abca4*$^{-/-}$ mice is not affected by the AAV-CRRY treatment. (A) Representative immunoblots of LC3-I (cytosolic), LC3-II (membrane bound), and α-tubulin using RPE homogenate (10 μg protein per lane) of Balb/*c* (top panel) and *Abca4*$^{-/-}$ (bottom panel) mice. **(B)** Histogram showing LC3 normalized protein data in the RPE homogenate samples shown in (A). RPE protein samples were obtained from 7-month-old *Abca4*$^{-/-}$ mice injected with AAV-CRRY or -Null viruses. Data presented as mean ± S.D. (n=4 mice per group; each protein sample was run in triplicate).

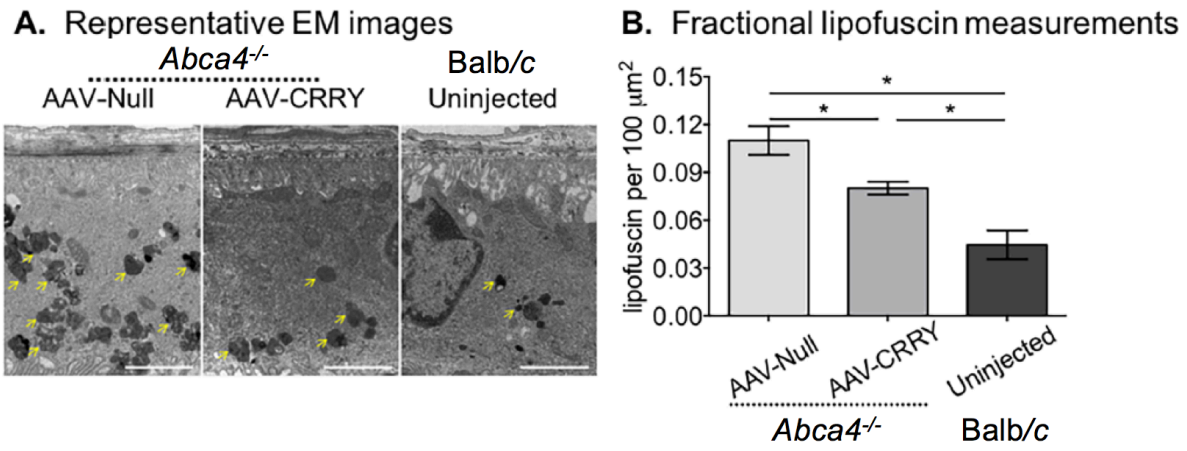

Figure 3.9. Lipofuscin accumulation is decreased in CRRY-injected *Abca4*$^{-/-}$ mice. (A) Representative electron microscopic images of RPE from 1-year-old *Abca4*$^{-/-}$ and Balb/*c* mice. Arrows indicate electron dense lipofuscin granules. Scale bar = 2 μm. **(B)** Histogram showing the lipofuscin fractional area measurements by electron microscopy. Data presented as mean ± S.D. (*p<0.005, n=4-11 mice per group).

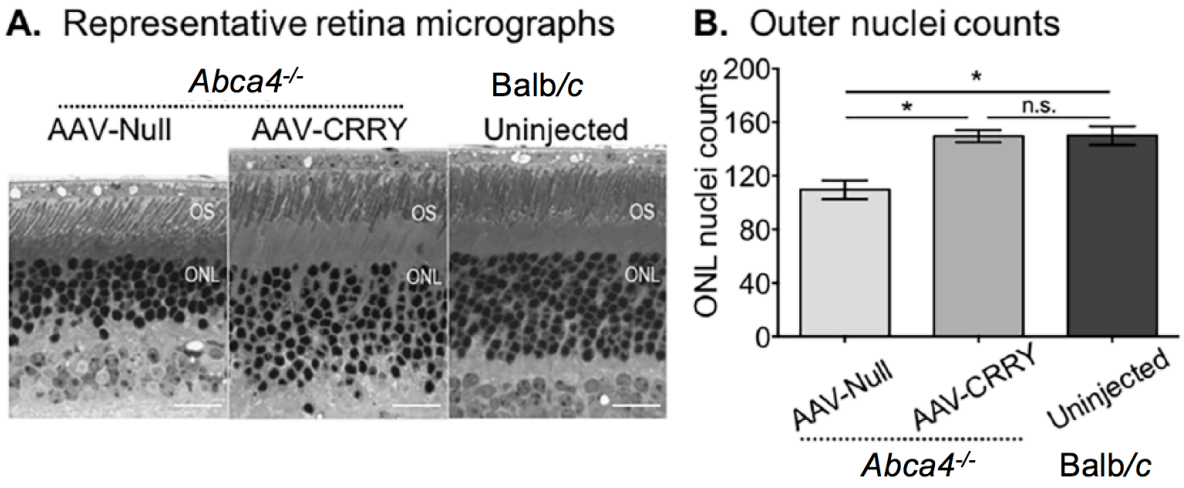

Figure 3.10. Rescue of photoreceptor cells in CRRY-injected *Abca4*$^{-/-}$ mice. (A) Representative light microscopic images of retinas from 1-year-old *Abca4*$^{-/-}$ and Balb/*c* mice. Scale bar = 20 μm. **(B)** Histogram showing the outer layer nuclei counts by light microscopy. Data presented as mean ± S.D. (**p*<0.005, n=5-9 mice).

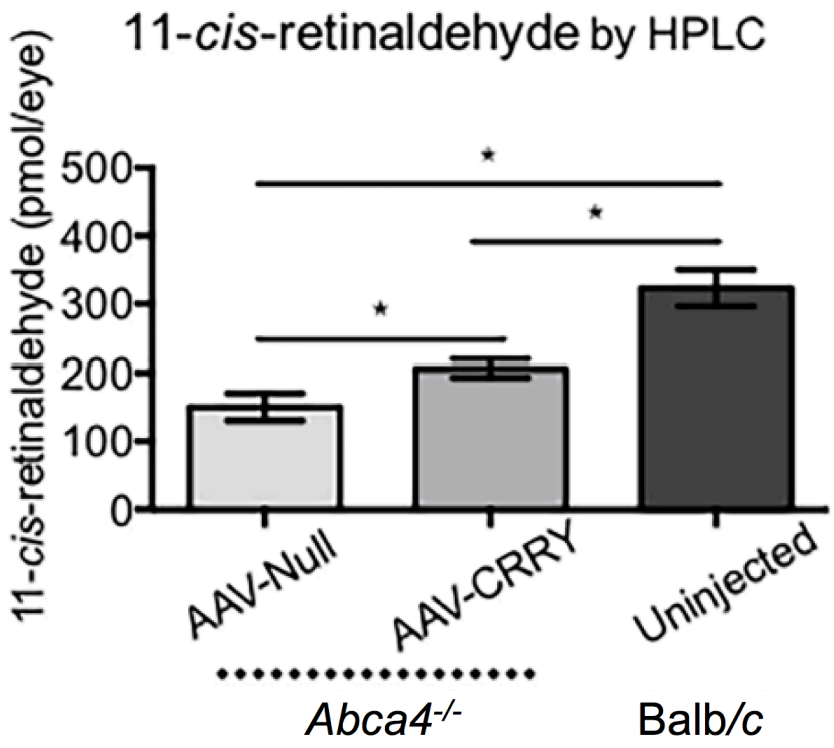

Figure 3.11. Visual chromophore (11-*cis*-retinaldehyde) is increased in CRRY-injected *Abca4-/-* mice. Retinoid levels were quantified by HPLC from hexane extracts of a single retina from 1-year-old *Abca4*$^{-/-}$ and Balb/*c* mice. 11-*cis*-retinaldehyde data is expressed as picomoles (pmol) per eye. Data presented as mean ± S.D. (n=6-8 mice per group; *p<0.005).

Chapter 4: Significance of cell-autonomous RPE dysfunction in STGD1

i. Expression of ABCA4 in the RPE and its implications for STGD1

RPE involvement in STGD1

STGD1 is the most common juvenile macular degeneration with an estimated worldwide prevalence of 1/8,000-1/10,000 and an average onset in the first two decades of life[15,16,96-98]. There is no cure for STGD1, which causes progressive central vision loss and delayed dark adaptation in young patients[99-103]. In addition to causing STGD1, ABCA4 mutations have also been associated with recessive cone-rod dystrophy, recessive retinitis pigmentosa, and increased susceptibility to AMD[104-109]. Research aimed at developing treatment for ABCA4-associated retinopathy currently encompasses gene replacement, stem cell therapy, and pharmacologic strategies[101,110-113]. Importantly, these approaches may be limited by the assumption that ABCA4 is exclusively expressed in retinal photoreceptor OS discs. The expression of ABCA4 in the RPE has not been extensively tested prior to this study, although expression of *ABCA4* outside of photoreceptors has in fact been indirectly shown in other tissues, including the RPE[18-21]. However, this dissertation describes the first evidence of expressed and functionally active ABCA4 protein in the RPE.

It is thought that RPE dysfunction plays an early pathogenic role and precedes photoreceptor cell loss in most STGD1 patients[38]. This may explain why some early presentations and mild, foveal-sparing variants of STGD1 present only with subtle changes in RPE autofluorescence intensity or texture[114-117]. Common findings in STGD1 include foveal atrophy surrounded by characteristic yellow flecks which are associated with initial hyperautofluorescence from lipofuscin accumulation at the level of the RPE[36,75,118-122]. Expansion of the bull's eye pattern hyperautofluorescent ring results in a hypoautofluorescent

wake due to subsequent cell death[39,123,124]. However, the wide phenotypic and genotypic heterogeneity in STGD1 has made it difficult to fully understand the complex interaction between RPE and photoreceptor degeneration[125,126]. The expression of ABCA4 in the RPE helps to clarify the cellular pathogenesis of STGD1, and thus also impacts future treatment strategies.

ABCA4 is expressed in the RPE, where it co-localizes with endo-phagolysosomal membranes

ABCA4 was previously thought to be present only in OS disks within ocular tissues, where it assists in processing retinaldehyde released following photoisomerization in rhodopsin. In the current work, we have shown that ABCA4 is additionally expressed in RPE cells, where it plays an important role in suppressing the phenotype in *Abca4*$^{-/-}$ mice and presumably STGD1 patients. The distal OS of rods and cones are shed and phagocytosed daily by RPE cells[24]. ABCA4 from photoreceptors may therefore be detectable in early RPE phagosomes before completion of OS proteolysis. We employed several approaches to control for the presence of photoreceptor-derived ABCA4 in RPE cells. The first was to look for ABCA4 mRNA in RPE cells. Since OS do not contain RNA, mRNA's present in RPE cells should be endogenously expressed. By RNA-Seq analysis and qRT-PCR, we found that the ABCA4 mRNA is present in RPE cells, similar to other RPE-expressed mRNA's including Rpe65, bestrophin, and LRAT (Fig. 1.1). In contrast, the mRNA's for proteins expressed specifically in photoreceptors, including rhodopsin, m-cone opsin and s-cone opsin, were undetectable or present at greatly reduced abundances in RPE (Fig. 1.1). These data indicate that the *ABCA4* gene is expressed in RPE cells.

Mertk$^{-/-}$ mice lack Mer tyrosine kinase, which is required for phagocytosis of OS by RPE cells[127]. *Mertk*$^{-/-}$ mice exhibit greatly impaired OS phagocytosis and degeneration of photoreceptors, which is complete by three months[26]. ABCA4 and RDS/peripherin are

membrane proteins located in the rims of rod and cone OS disks[3-5,8,128,129]. ABCA4 and RDS/peripherin were present in five-month-old wild type retina and RPE homogenates, but undetectable in *Mertk*$^{-/-}$ retinas of the same age (Figs. 1.2A and 1.2B), consistent with complete degeneration of photoreceptors in these animals. Importantly, ABCA4 was present at ~20% of the wild type level in *Mertk*$^{-/-}$ RPE homogenates, while RDS/peripherin was nearly undetectable in the same samples. The presence of ABCA4 immunoreactivity in RPE homogenates from fully degenerate *Mertk*$^{-/-}$ mice suggests that the ABCA4 protein is endogenously expressed in the RPE.

We also tested for ABCA4 expression in RPE cells by immunofluorescence analysis. Wild type (129/Sv) retinas showed ABCA4 immunofluorescence in photoreceptor OS and RPE cells, while degenerate *Mertk*$^{-/-}$ sections showed ABCA4 immunofluorescence only in the RPE (Fig. 1.3A). As expected, we observed no ABCA4 immunofluorescence in *Abca4*$^{-/-}$ retina/RPE sections (Fig. 1.3A). Human RPE precursor cells were collected from fetal retinas before appearance of OS[27], and hence were never exposed to exogenous ABCA4. Immunofluorescence analysis on sections of hfRPE cells grown to confluence showed a granular pattern of ABCA4 immunoreactivity, consistent with a distribution in internal membranes (Fig. 1.3B). The presence of ABCA4 immunoreactivity in *Mertk*$^{-/-}$ RPE cells, which are incapable of OS phagocytosis, and in hfRPE cells, which were never exposed to photoreceptor OS, confirms that ABCA4 is expressed in RPE cells. Co-localization of ABCA4 with CAV1 and LAMP1 inside RPE cells (Figs. 1.3C and 1.3D) suggests that ABCA4 is present in endo-phagolysosomal membranes.

Transgenic RPE-specific expression of ABCA4 in Abca4$^{-/-}$ *mice improves the Abca4*$^{-/-}$ *phenotype*

The phenotype in albino *Abca4*$^{-/-}$ mice includes accumulation of bisretinoid pigments such as A2E in the RPE, deposition of fluorescent lipofuscin granules in RPE cells, and slow photoreceptor degeneration. To what extent does this phenotype depend on loss of ABCA4 from RPE cells? We addressed this question by expressing ABCA4 in the RPE of transgenic *Abca4*$^{-/-}$ mice. These *RPE-Abca4-Tg/Abca4*$^{-/-}$ mice expressed the ABCA4 protein in the RPE at approximately 20% the level in wild type RPE, with no detectable expression of ABCA4 in photoreceptors (Fig. 2.3). Notwithstanding this low expression of ABCA4 in the RPE, we observed 50% slowing of A2E accumulation in *RPE-Abca4-Tg/Abca4*$^{-/-}$ versus non-transgenic *Abca4*$^{-/-}$ mice (Fig. 2.4A). In addition to the improved A2E profile measured by HPLC, we saw similarly consistent improvements in RPE lipofuscin burden and RPE autofluorescence (Fig. 2.5). Photoreceptor degeneration was also slowed by 50% in the transgenic versus non-transgenic *Abca4*$^{-/-}$ mice (Fig. 2.6A-B). Thus, expression of ABCA4 in RPE at only 20% the level in wild type mice yielded 50% rescue of lipofuscin accumulation and photoreceptor degeneration. Expression of ABCA4 in the RPE at levels nearer to wild type would probably deliver still greater rescue of the *Abca4*$^{-/-}$ phenotype. Interestingly, levels of the bisretinoids: A2PE, A2PE-H_2, and all-*trans*-RAL-dimer in the retinas of *Abca4*$^{-/-}$ mice were less affected by transgenic expression of ABCA4 in the RPE (Figs. 2.4B-D). These bisretinoids probably formed due to loss of ABCA4 in photoreceptor OS. The observed 50% slowing of photoreceptor degeneration in *RPE-Abca4-Tg/Abca4*$^{-/-}$ versus *Abca4*$^{-/-}$ mice despite similar levels of bisretinoids in their retinas, suggests that ABCA4 in the RPE is critical to the preservation of photoreceptors.

Despite any modest “rescue” effects seen with replacement of RPE-expressed ABCA4, greater improvements would certainly be anticipated if photoreceptor-expressed ABCA4 was also replaced. However, given that the majority of ABCA4 is expressed in the retina, and not the RPE, the effects seen in this study are appropriate, reflecting mild improvement due to the

physiologic relationship between the RPE and the photoreceptors. For example, although a functional difference in scotopic *a*-wave amplitude was seen between wild type and *Abca4*$^{-/-}$ mice, the transgenic model most likely did not show significant functional improvement because the photoreceptors were not directly rescued (Fig. 2.7).

Proposed physiologic role of ABCA4 in RPE cells

Given that ABCA4 co-localizes with the membrane associated proteins LAMP1 and CAV1 in lysosomes and endo-phagolysosomes respectively, we propose that ABCA4 acts as a flippase within the endo-phagolysosomal membrane network in RPE cells (Fig. 2.1). Following daily phagocytosis of the distal 10% of photoreceptor outer segments, rhodopsin and cone opsins are taken up by the RPE and proteolysed, releasing free 11-*cis*-RAL into the phagolysosome where it readily reacts with phosphatidylethanolamine (PE) in the membrane to form 11-*cis*-*N*-ret-PE. A fraction of this material may isomerize (thermally or light-induced) to form all-*trans*-*N*-ret-PE, and both isomers of *N*-ret-PE would be available to RPE-expressed ABCA4 in endo-phagolysosomal membranes, across which they would be flipped to the cytoplasmic surface, maintaining the same directionality proposed by ABCA4 flippase in photoreceptor OS[11]. Following translocation to the RPE cytoplasm, spontaneous hydrolysis of *N*-ret-PE would then yield free 11-*cis*-RAL or all-*trans*-RAL, which would contribute to opsin pigment regeneration via either CRALBP-mediated export of 11-*cis*-RAL back to the photoreceptor, or retinol dehydrogenase type-10 (RDH10)-mediated reduction of all-*trans*-RAL to all-*trans*-retinol for recycling of visual pigment[130-133]. Thus, the proposed function of ABCA4 in the RPE, to accelerate the transfer of *N*-ret-PE from the luminal to cytoplasmic leaflet of endo-phagolysosomal membranes for chromophore recycling, is similar to the activity of ABCA4 in OS disc membranes.

Bisretinoids may form directly in the RPE

It was previously thought that bisretinoids only formed from light-activated all-*trans*-RAL in photoreceptors, and became secondarily deposited in the RPE by phagocytosis, or as a recent study suggested, delivered to the RPE by activated microglia[134]. It was surprising then that *Abca4*$^{-/-}$ mice raised in total darkness (with presumably less release of photoactivated all-*trans*-RAL), still accumulate similar levels of A2E as cyclic light-reared mice[50]. Although small amounts of thermal isomerization from 11-*cis*-RAL to all-*trans*-RAL do occur, these negligible levels of free thermally produced free all-*trans*-RAL could not account for the high levels of RPE bisretinoids that were surprisingly seen in dark-reared *Abca4*$^{-/-}$ mice. Instead, the study authors attributed the 'dark-reared' bisretinoids to 11-*cis*-RAL, as opposed to all-*trans*-RAL, as the primary substrate. According to this model, the visual cycle continues to supply photoreceptors with 11-*cis*-RAL in the dark. This unused 11-*cis*-RAL forms 11-*cis*-*N*-ret-PE, which is normally transported out of the disks by ABCA4. In *Abca4*$^{-/-}$ mice lacking this flippase, the 11-*cis*-*N*-ret-PE condenses with another 11-*cis*-RAL to form an iso-bisretinoid, which is converted to lipofuscin in the RPE after OS phagocytosis. The problem with this model is that synthesis of visual chromophore by the RPE requires the presence of apo-CRALBP, as a mechanism to match 11-*cis*-RAL synthesis with the demand for chromophore[135]. Once all visual pigments are regenerated, excess 11-*cis*-RAL binds to CRALBP, saturating it with ligand and arresting further synthesis. Consistently, dark-adapted mouse retinas were shown to contain only 10 pmols of 11-*cis*-*N*-ret-PE versus 450 pmols of 11-*cis*-RAL in rhodopsin[136]. For this reason, removal of excess 11-*cis*-RAL by ABCA4 in OS is unlikely to explain the accumulation of A2E in dark-reared animals. A more likely function for ABCA4 in the dark is to clear retinaldehydes released during visual-pigment proteolysis in RPE phagolysosomes following phagocytosis of distal OS. Thus, an alternative explanation for 'dark-reared' bisretinoids could be that they are formed directly in the RPE from either 11-*cis*-RAL or all-*trans*-RAL.

Another question posed in recent literature is why *Mertk*$^{-/-}$ mice, which are left with RPE but no photoreceptors due to a defect in phagocytosis, retain high A2E levels[134]. If bisretinoids are indeed forming directly in the RPE, this could explain several unanswered questions in the literature such as the conundrum of "dark-reared bisretinoids" and "*Mertk*$^{-/-}$ bisretinoids." Our finding, that RPE-expressed ABCA4 plays a role in reducing bisretinoid burden in the RPE, provides evidence that free retinaldehydes in the RPE are a primary and direct source of bisretinoid formation.

Potential downstream consequences of ABCA4 loss in RPE

Mechanistically, our research supports previous studies that have implicated complement dysregulation in the pathogenesis of STGD1. A2E has been shown to exert cytotoxic effects through a variety of different and possibly linked mechanisms (oxidative stress, lysosomal dysfunction, disrupted autophagy, interference with cholesterol metabolism) [52-64]. Complement dysregulation is strongly implicated in the pathogenesis of *Abca4*$^{-/-}$ mice and STGD1 patients[52,57], as well as in AMD patients which share similar phenotypic features such as lipofuscin accumulation[77-83]. Our study confirmed previous findings[52] that activation of complement is significantly higher in *Abca4*$^{-/-}$ RPE compared to wild type RPE, as evidenced by C3b accumulation on Western blot (Fig. 2.8). Importantly, the *RPE-Abca4-Tg/Abca4*$^{-/-}$ RPE showed improved levels of C3b accumulation, suggesting that the presence of RPE-expressed ABCA4 plays a protective role in curbing complement dysregulation.

Impact of RPE-expressed ABCA4 in emerging therapeutics for STGD1

Our demonstration that ABCA4 is expressed in the RPE, and that loss of ABCA4 from these cells is responsible for much of the phenotype in *Abca4*$^{-/-}$ mice, has important implications for the treatment of *ABCA4*-mediated macular and retinal degenerations. These diseases

include STGD1, approximately one third of recessive cone-rod dystrophy[108], and a small subset of recessive retinitis pigmentosa[109]. One treatment approach is gene therapy. If ABCA4 were only expressed in photoreceptor OS, as previously thought, treatment would require efficient transduction of photoreceptors by a recombinant virus containing the 6.8-kb *ABCA4* coding region. However, photoreceptors are only transduced at low efficiencies[137,138]. The current results suggest that viral transduction of photoreceptors is not required. We observed two-fold reductions in the critical parameters of A2E accumulation and photoreceptor degeneration (Figs. 2.4 and 2.6) by expressing ABCA4 in RPE but not photoreceptors of *Abca4*$^{-/-}$ mice. Further, the level of ABCA4 protein in these cells was only about 20% of the wild type level (Fig. 2.3). In contrast to photoreceptors, recombinant viruses transduce RPE cells at high efficiency, often with levels of protein expression exceeding the level observed here. Thus, RPE cells are far more tractable than photoreceptors as targets for gene therapy of *ABCA4*-mediated retinopathies. A second treatment approach is cell transplantation. Here again, expression of ABCA4 in RPE cells opens therapeutic possibilities. Induced pluripotent stem cells (iPSC's) can be readily programed to become functional RPE cells. Numerous studies have shown successful transplantation of iPSC-derived RPE cells into the subretinal space of animals and humans[113,139]. Targeted gene editing of patient-derived iPSC's could be used to correct mutations in *ABCA4*, allowing for autologous transplants of functional RPE cells. Still a third treatment approach is intraocular delivery of pharmacologic agents that target formation of toxic lipofuscin pigments. Here again, the high uptake capacity of RPE cells would assist in the delivery of drugs to their cellular target.

In summary, we have shown in Chapter 1 that ABCA4 is expressed in RPE cells, and in Chapter 2 that much of the phenotype in *Abca4*$^{-/-}$ mice is caused by loss of RPE-expressed ABCA4. These observations change the prime cellular target for treatment of *ABCA4*-mediated retinopathies from photoreceptors to the more tractable RPE cells. These findings provide

rational support to treatments involving *ABCA4* gene therapy, RPE cell-transplantation, and intraocular delivery of new drugs targeting RPE cells.

ii. Complement modulation in the RPE rescues photoreceptor degeneration in a mouse model of Stargardt disease

Complement dysregulation in AMD and STGD1

The complement system, a key component of innate immunity, is necessary to maintain tissue homeostasis. In the eye, the RPE plays a major role in controlling the immune response through expression of various complement regulators, or CRPs. Accumulation of bisretinoid pigments in the RPE is a characteristic feature of STGD1 and the *Abca4*$^{-/-}$ mouse[33,52]. The association between bisretinoids and complement activation has been well established in cultured RPE cells[57,76,140] and in *Abca4*$^{-/-}$ mice[52]. Further, the complement factor F (CFH) gene which encodes a soluble CRP secreted by RPE cells[141], is an important susceptibility locus for AMD, a disease with significant similarities to STGD1[84]. Complement activation in bisretinoid-laden RPE cells was strongly dependent on the *CFH* haplotype[140]. Finally, cellular protective mechanisms against sublytic complement deposition have been shown to be impaired in *Abca4*$^{-/-}$ mice[70]. These findings suggest that RPE cells become unable to protect themselves from sub-lethal attack by the complement system as they accumulate bisretinoid pigments, resulting in RPE dysfunction and photoreceptor degeneration.

Viral gene therapy-mediated overexpression of a major complement regulatory protein improves the Abca4$^{-/-}$ *phenotype*

In this study, we attempted to protect cells against complement attack by increasing expression of a major CRP of the alternative complement pathway, CRRY, in the RPE of *Abca4*$^{-}$

$^{-/-}$ mice. The human homolog of CRRY is membrane cofactor protein (MCP), also known as CD46, which is implicated in several diseases including AMD[142]. A single subretinal injection of AAV-CRRY in 4-week-old *Abca4*$^{-/-}$ mice was sufficient to sustain a several-fold increase in CRRY expression in the RPE beyond one year without affecting the levels of other CRPs (Fig. 3.2). CRRY prevents cleavage of complement components C3 and C5, which generate reactive fragments and subsequently form the cytolytic membrane attack complex (MAC)[143]. The MAC proteins deposit on the plasma membrane of RPE cells to create a sublytic complex that degrades RPE function without killing the cell[144,145]. MCP is expressed in the basolateral membranes of human RPE cells, where it is exposed to the choroidal circulation. MCP and CRRY bind complement C3b with high affinity, inhibiting the C3 convertase amplification loop that leads to MAC deposition [146]. Here we show that CRRY overexpression in AAV-CRRY-injected *Abca4*$^{-/-}$ eyes leads to reduced deposition of the C3 breakdown fragments, C3b and iC3b (Fig. 3.3).

The presence of reactive complement proteins on the surface of RPE cells may accelerate lipofuscin accumulation by impeding its clearance via endo-phagolysosomes within the RPE[147]. This concept is supported by the observation that the RPE region transduced by the AAV-CRRY virus exhibited decreased autofluorescence (Fig. 3.4). In the case of STGD1 patients and *Abca4*$^{-/-}$ mice, this autofluorescent material contains abundant A2E and related bisretinoids[33,148]. Bisretinoid levels in RPE homogenates of the AAV-CRRY-injected group were ~two-fold lower compared to the AAV-Null-injected group (Fig. 4). These data lend further support to the association between complement activation and buildup of vitamin A byproducts in RPE cells. Increased bisretinoid-lipofuscin granules within RPE cells have been shown to inhibit cholesterol-mediated autophagy[71]. We measured levels of LC3, a key marker of autophagy, in response to AAV-CRRY injection. Although the relative amount of LC3 was significantly lower in the *Abca4*$^{-/-}$ mice compared to the wild type group, similar levels of LC3

were observed in mice that received AAV-CRRY and AAV-null virus injections (Fig. 3.8). Likewise, anti-oxidative stress protein levels were similar for AAV-CRRY-injected and AAV-Null injected *Abca4*$^{-/-}$ mice (Fig. 3.7). These data suggest that even mild accumulations of bisretinoid above wild type levels was sufficient to induce cellular stress.

A major effect of increasing CRRY expression in the RPE of the *Abca4*$^{-/-}$ mice was the slowing of photoreceptor degeneration (Fig. 3.10). We observed about 30% increase in the number of photoreceptor nuclei in the area transduced by the AAV-CRRY treatment. This modest but significant rescue was evidenced by increased visual chromophore in AAV-CRRY treated *Abca4*$^{-/-}$ mice (Fig. 3.11). In *Abca4*$^{-/-}$ mice and STGD1 patients, photoreceptor degeneration is attributed to bisretinoid accumulation by the RPE[33,38]. With time, the combination of bisretinoid accumulation and complement activation may impair the recycling of retinoids released from phagocytosed OS in the RPE. This favors the formation of bisretinoids such as A2E[88]. Reduced bisretinoid levels were observed in *Abca4*$^{-/-}$ mice treated with drugs that lower circulating vitamin A or inhibit enzymes of the visual cycle[85,90,149]. Combination drug therapy with both complement modulators and visual cycle inhibitors may be an effective treatment strategy for STGD1 since it targets both pathogenic mechanisms.

Reducing inappropriate complement activation as a treatment approach for STGD1

Rescue of both bisretinoid accumulation and photoreceptor degeneration by subretinal injection of AAV-CRRY suggests that inappropriate activation of the complement cascade plays a role in the pathogenesis STGD1. Correlation between mono-allelic sequence variants in the *ABCA4* gene and a clinically distinct subset of 'dry' AMD patients[150], together with the current findings, suggest a common final etiological pathway for STGD1 and some cases of AMD[150]. In AMD, complement dysfunction in the RPE can be caused by mutations in the gene for CFH or other complement regulatory proteins[81,83,151,152]. In contrast, the primary defect in STGD1 is loss

of the ABCA4 transporter, which is responsible for the formation and accumulation of toxic bisretinoids in the RPE[17,33]. Degeneration of macular photoreceptors in both diseases results from loss of RPE support. Our study shows that normalizing local complement activity in aged or diseased RPE may prolong photoreceptor viability.

iii. Conclusion

Chapter 1 of this dissertation provides the first direct evidence that ABCA4 is expressed in the RPE, within endo-phagolysosomal structures. Here, ABCA4 plays a similar role in RPE internal membranes as it does in photoreceptor OS discs, that is, to recycle free retinaldehydes.

Through characterization of a transgenic mouse model expressing ABCA4 in the RPE, but not in photoreceptors, Chapter 2 reveals that RPE-expressed ABCA4 confers cytoprotection against bisretinoid induced complement dysregulation. This study suggests that bisretinoid formation may be occurring directly in the RPE, not just in the photoreceptor with secondary deposition in the RPE. Thus, transgenic overexpression of ABCA4 uniquely in the RPE on the *Abca4*$^{-/-}$ background resulted in relative rescue: reduced accumulation of visual cycle toxic byproducts, decreased complement dysfunction, and improvement in late-onset photoreceptor degeneration.

Finally, Chapter 3 identifies that inappropriate activation of the complement cascade plays a role in the pathogenesis of recessive Stargardt macular degeneration. We showed in *Abca4*$^{-/-}$ mice that over-expression of CRRY, a major murine CRP, reduces complement attack on the RPE and rescues both bisretinoid accumulation and photoreceptor degeneration.

In summary, this work introduces a cell-autonomous disease process in Stargardt disease and may direct future targeted therapies for ABCA4-associated disease as well as related maculopathies involving complement dysregulation.

References:

1 Wald, G. The molecular basis of visual excitation. *Nature* **219**, 800-807 (1968).

2 Kiser, P. D., Golczak, M. & Palczewski, K. Chemistry of the retinoid (visual) cycle. *Chemical reviews* **114**, 194-232, doi:10.1021/cr400107q (2014).

3 Papermaster, D. S., Schneider, B. G., Zorn, M. A. & Kraehenbuhl, J. P. Immunocytochemical localization of a large intrinsic membrane protein to the incisures and margins of frog rod outer segment disks. *The Journal of cell biology* **78**, 415-425 (1978).

4 Illing, M., Molday, L. L. & Molday, R. S. The 220-kDa rim protein of retinal rod outer segments is a member of the ABC transporter superfamily. *The Journal of biological chemistry* **272**, 10303-10310 (1997).

5 Sun, H. & Nathans, J. Stargardt's ABCR is localized to the disc membrane of retinal rod outer segments. *Nature genetics* **17**, 15-16, doi:10.1038/ng0997-15 (1997).

6 Azarian, S. M. & Travis, G. H. The photoreceptor rim protein is an ABC transporter encoded by the gene for recessive Stargardt's disease (ABCR). *FEBS letters* **409**, 247-252 (1997).

7 Sun, H., Molday, R. S. & Nathans, J. Retinal stimulates ATP hydrolysis by purified and reconstituted ABCR, the photoreceptor-specific ATP-binding cassette transporter responsible for Stargardt disease. *The Journal of biological chemistry* **274**, 8269-8281 (1999).

8 Molday, L. L., Rabin, A. R. & Molday, R. S. ABCR expression in foveal cone photoreceptors and its role in Stargardt macular dystrophy. *Nature genetics* **25**, 257-258, doi:10.1038/77004 (2000).

9 Ahn, J., Wong, J. T. & Molday, R. S. The effect of lipid environment and retinoids on the ATPase activity of ABCR, the photoreceptor ABC transporter responsible for Stargardt

macular dystrophy. *The Journal of biological chemistry* **275**, 20399-20405, doi:10.1074/jbc.M000555200 (2000).

10 Beharry, S., Zhong, M. & Molday, R. S. N-retinylidene-phosphatidylethanolamine is the preferred retinoid substrate for the photoreceptor-specific ABC transporter ABCA4 (ABCR). *The Journal of biological chemistry* **279**, 53972-53979, doi:10.1074/jbc.M405216200 (2004).

11 Quazi, F., Lenevich, S. & Molday, R. S. ABCA4 is an N-retinylidene-phosphatidylethanolamine and phosphatidylethanolamine importer. *Nature communications* **3**, 925, doi:10.1038/ncomms1927 (2012).

12 Weng, J. *et al.* Insights into the function of Rim protein in photoreceptors and etiology of Stargardt's disease from the phenotype in abcr knockout mice. *Cell* **98**, 13-23, doi:10.1016/S0092-8674(00)80602-9 (1999).

13 Molday, R. S., Zhong, M. & Quazi, F. The role of the photoreceptor ABC transporter ABCA4 in lipid transport and Stargardt macular degeneration. *Biochimica et biophysica acta* **1791**, 573-583, doi:10.1016/j.bbalip.2009.02.004 (2009).

14 Sahu, B. & Maeda, A. Retinol Dehydrogenases Regulate Vitamin A Metabolism for Visual Function. *Nutrients* **8**, doi:10.3390/nu8110746 (2016).

15 Stargardt, K. Ueber familiare, progressive Degeneration in der Makulagegend des Auges. *Albrecht Von Graefes Arch Klin Exp Ophthalmol*, 534-549 (1909).

16 Blacharski, P. A. in *Retinal dystropies and degernations* (ed D. A. Newsome) 135-139 (Raven Press, 1988).

17 Allikmets, R. *et al.* A photoreceptor cell-specific ATP-binding transporter gene (ABCR) is mutated in recessive Stargardt macular dystrophy. *Nature genetics* **15**, 236-246, doi:10.1038/ng0397-236 (1997).

18 Bhongsatiern, J., Ohtsuki, S., Tachikawa, M., Hori, S. & Terasaki, T. Retinal-specific ATP-binding cassette transporter (ABCR/ABCA4) is expressed at the choroid plexus in rat brain. *J Neurochem* **92**, 1277-1280, doi:10.1111/j.1471-4159.2004.02941.x (2005).

19 Wiley, L., Kaalberg, E., Mullins, R., Stone, E. & Tucker, B. Expression of the retina-specific flippase, ABCA4, in epidermal keratinocytes [version 1; referees: 2 approved with reservations]. *F1000 Research* **5**, 193 (2016).

20 Zhang, Z. *et al.* A gene expression profile of the developing human retinal pigment epithelium. *Molecular vision* **18**, 2961-2975 (2012).

21 Radeke, M. J. *et al.* Restoration of mesenchymal retinal pigmented epithelial cells by TGFbeta pathway inhibitors: implications for age-related macular degeneration. *Genome Med* **7**, 58, doi:10.1186/s13073-015-0183-x (2015).

22 Strauss, O. The retinal pigment epithelium in visual function. *Physiol Rev* **85**, 845-881, doi:10.1152/physrev.00021.2004 (2005).

23 Young, R. W. The renewal of photoreceptor cell outer segments. *The Journal of cell biology* **33**, 61-72 (1967).

24 Young, R. W. & Bok, D. Participation of the retinal pigment epithelium in the rod outer segment renewal process. *The Journal of cell biology* **42**, 392-403 (1969).

25 LaVail, M. M. Rod outer segment disk shedding in rat retina: relationship to cyclic lighting. *Science* **194**, 1071-1074 (1976).

26 Duncan, J. L. *et al.* An RCS-like retinal dystrophy phenotype in mer knockout mice. *Investigative ophthalmology & visual science* **44**, 826-838 (2003).

27 Hu, J. & Bok, D. Culture of highly differentiated human retinal pigment epithelium for analysis of the polarized uptake, processing, and secretion of retinoids. *Methods in molecular biology* **652**, 55-73, doi:10.1007/978-1-60327-325-1_2 (2010).

28 Sethna, S. *et al.* Regulation of Phagolysosomal Digestion by Caveolin-1 of the Retinal Pigment Epithelium Is Essential for Vision. *The Journal of biological chemistry* **291**, 6494-6506, doi:10.1074/jbc.M115.687004 (2016).

29 Hu, J. & Bok, D. A cell culture medium that supports the differentiation of human retinal pigment epithelium into functionally polarized monolayers. *Molecular vision* **7**, 14-19 (2001).

30 Kedzierski, W., Bok, D. & Travis, G. H. Transgenic analysis of rds/peripherin N-glycosylation: effect on dimerization, interaction with rom1, and rescue of the rds null phenotype. *J Neurochem* **72**, 430-438 (1999).

31 Johnson, L. V. *et al.* Cell culture model that mimics drusen formation and triggers complement activation associated with age-related macular degeneration. *Proceedings of the National Academy of Sciences of the United States of America* **108**, 18277-18282, doi:10.1073/pnas.1109703108 (2011).

32 Mata, N. L. *et al.* Delayed dark-adaptation and lipofuscin accumulation in abcr+/- mice: implications for involvement of ABCR in age-related macular degeneration. *Investigative ophthalmology & visual science* **42**, 1685-1690 (2001).

33 Mata, N. L., Weng, J. & Travis, G. H. Biosynthesis of a major lipofuscin fluorophore in mice and humans with ABCR-mediated retinal and macular degeneration. *Proceedings of the National Academy of Sciences of the United States of America* **97**, 7154-7159, doi:10.1073/pnas.130110497 (2000).

34 Feeney-Burns, L., Hilderbrand, E. S. & Eldridge, S. Aging human RPE: morphometric analysis of macular, equatorial, and peripheral cells. *Investigative ophthalmology & visual science* **25**, 195-200 (1984).

35 De Laey, J. J. & Verougstraete, C. Hyperlipofuscinosis and subretinal fibrosis in Stargardt's disease. *Retina* **15**, 399-406 (1995).

36 Delori, F. C. *et al.* In vivo fluorescence of the ocular fundus exhibits retinal pigment epithelium lipofuscin characteristics. *Investigative ophthalmology & visual science* **36**, 718-729 (1995).

37 Cideciyan, A. V. *et al.* Reduced-illuminance autofluorescence imaging in ABCA4-associated retinal degenerations. *J Opt Soc Am A Opt Image Sci Vis* **24**, 1457-1467 (2007).

38 Cideciyan, A. V. *et al.* Mutations in ABCA4 result in accumulation of lipofuscin before slowing of the retinoid cycle: a reappraisal of the human disease sequence. *Human molecular genetics* **13**, 525-534, doi:10.1093/hmg/ddh048 (2004).

39 Cukras, C. A. *et al.* Centrifugal expansion of fundus autofluorescence patterns in Stargardt disease over time. *Archives of ophthalmology* **130**, 171-179, doi:10.1001/archophthalmol.2011.332 (2012).

40 Kennedy, C. J., Rakoczy, P. E. & Constable, I. J. Lipofuscin of the retinal pigment epithelium: a review. *Eye* **9 (Pt 6)**, 763-771, doi:10.1038/eye.1995.192 (1995).

41 Brunk, U. T. & Terman, A. Lipofuscin: mechanisms of age-related accumulation and influence on cell function. *Free radical biology & medicine* **33**, 611-619 (2002).

42 Katz, M. L., Drea, C. M. & Robison, W. G., Jr. Relationship between dietary retinol and lipofuscin in the retinal pigment epithelium. *Mech Ageing Dev* **35**, 291-305 (1986).

43 Katz, M. L., Eldred, G. E. & Robison, W. G., Jr. Lipofuscin autofluorescence: evidence for vitamin A involvement in the retina. *Mech Ageing Dev* **39**, 81-90 (1987).

44 Katz, M. L. & Redmond, T. M. Effect of Rpe65 knockout on accumulation of lipofuscin fluorophores in the retinal pigment epithelium. *Investigative ophthalmology & visual science* **42**, 3023-3030 (2001).

45 Eldred, G. E. & Lasky, M. R. Retinal age pigments generated by self-assembling lysosomotropic detergents. *Nature* **361**, 724-726, doi:10.1038/361724a0 (1993).

46 Katz, M. L., Gao, C. L. & Rice, L. M. Formation of lipofuscin-like fluorophores by reaction of retinal with photoreceptor outer segments and liposomes. *Mech Ageing Dev* **92**, 159-174 (1996).

47 Ben-Shabat, S. *et al.* Biosynthetic studies of A2E, a major fluorophore of retinal pigment epithelial lipofuscin. *The Journal of biological chemistry* **277**, 7183-7190, doi:10.1074/jbc.M108981200 (2002).

48 Sparrow, J. R. & Boulton, M. RPE lipofuscin and its role in retinal pathobiology. *Experimental eye research* **80**, 595-606, doi:10.1016/j.exer.2005.01.007 (2005).

49 Charbel Issa, P. *et al.* Fundus Autofluorescence in the Abca4(−/−) Mouse Model of Stargardt Disease—Correlation With Accumulation of A2E, Retinal Function, and Histology. *Investigative ophthalmology & visual science* **54**, 5602-5612 (2013).

50 Boyer, N. P. *et al.* Lipofuscin and N-retinylidene-N-retinylethanolamine (A2E) accumulate in retinal pigment epithelium in absence of light exposure: their origin is 11-cis-retinal. *The Journal of biological chemistry* **287**, 22276-22286, doi:10.1074/jbc.M111.329235 (2012).

51 Delori, F. C. *et al.* In vivo measurement of lipofuscin in Stargardt's disease--Fundus flavimaculatus. *Investigative ophthalmology & visual science* **36**, 2327-2331 (1995).

52 Radu, R. A. *et al.* Complement system dysregulation and inflammation in the retinal pigment epithelium of a mouse model for Stargardt macular degeneration. *The Journal of biological chemistry* **286**, 18593-18601, doi:10.1074/jbc.M110.191866 (2011).

53 Holz, F. G. *et al.* Inhibition of lysosomal degradative functions in RPE cells by a retinoid component of lipofuscin. *Investigative ophthalmology & visual science* **40**, 737-743 (1999).

54 Sparrow, J. R., Cai, B., Jang, Y. P., Zhou, J. & Nakanishi, K. A2E, a fluorophore of RPE lipofuscin, can destabilize membrane. *Advances in experimental medicine and biology* **572**, 63-68, doi:10.1007/0-387-32442-9_10 (2006).

55 Sparrow, J. R., Parish, C. A., Hashimoto, M. & Nakanishi, K. A2E, a lipofuscin fluorophore, in human retinal pigmented epithelial cells in culture. *Investigative ophthalmology & visual science* **40**, 2988-2995 (1999).

56 Sparrow, J. R., Nakanishi, K. & Parish, C. A. The lipofuscin fluorophore A2E mediates blue light-induced damage to retinal pigmented epithelial cells. *Investigative ophthalmology & visual science* **41**, 1981-1989 (2000).

57 Zhou, J., Jang, Y. P., Kim, S. R. & Sparrow, J. R. Complement activation by photooxidation products of A2E, a lipofuscin constituent of the retinal pigment epithelium. *Proceedings of the National Academy of Sciences of the United States of America* **103**, 16182-16187, doi:10.1073/pnas.0604255103 (2006).

58 Sparrow, J. R. *et al.* A2E-epoxides damage DNA in retinal pigment epithelial cells. Vitamin E and other antioxidants inhibit A2E-epoxide formation. *The Journal of biological chemistry* **278**, 18207-18213, doi:10.1074/jbc.M300457200 (2003).

59 Sparrow, J. R., Zhou, J. & Cai, B. DNA is a target of the photodynamic effects elicited in A2E-laden RPE by blue-light illumination. *Investigative ophthalmology & visual science* **44**, 2245-2251 (2003).

60 Finnemann, S. C., Leung, L. W. & Rodriguez-Boulan, E. The lipofuscin component A2E selectively inhibits phagolysosomal degradation of photoreceptor phospholipid by the retinal pigment epithelium. *Proceedings of the National Academy of Sciences of the United States of America* **99**, 3842-3847, doi:10.1073/pnas.052025899 (2002).

61 Vives-Bauza, C. *et al.* The age lipid A2E and mitochondrial dysfunction synergistically impair phagocytosis by retinal pigment epithelial cells. *The Journal of biological chemistry* **283**, 24770-24780, doi:10.1074/jbc.M800706200 (2008).

62 Lakkaraju, A. Endo-lysosome function in the retinal pigment epithelium in health and disease. *Advances in experimental medicine and biology* **723**, 723-729, doi:10.1007/978-1-4614-0631-0_92 (2012).

63 Radu, R. A., Mata, N. L., Bagla, A. & Travis, G. H. Light exposure stimulates formation of A2E oxiranes in a mouse model of Stargardt's macular degeneration. *Proceedings of the National Academy of Sciences of the United States of America* **101**, 5928-5933, doi:10.1073/pnas.0308302101 (2004).

64 Bergmann, M., Schutt, F., Holz, F. G. & Kopitz, J. Inhibition of the ATP-driven proton pump in RPE lysosomes by the major lipofuscin fluorophore A2-E may contribute to the pathogenesis of age-related macular degeneration. *FASEB J* **18**, 562-564, doi:10.1096/fj.03-0289fje (2004).

65 Katz, M. L., Drea, C. M., Eldred, G. E., Hess, H. H. & Robison, W. G., Jr. Influence of early photoreceptor degeneration on lipofuscin in the retinal pigment epithelium. *Experimental eye research* **43**, 561-573 (1986).

66 Katz, M. L. & Eldred, G. E. Retinal light damage reduces autofluorescent pigment deposition in the retinal pigment epithelium. *Investigative ophthalmology & visual science* **30**, 37-43 (1989).

67 Feeney-Burns, L. & Eldred, G. E. The fate of the phagosome: conversion to 'age pigment' and impact in human retinal pigment epithelium. *Trans Ophthalmol Soc U K* **103 (Pt 4)**, 416-421 (1983).

68 Yau, K. W., Matthews, G. & Baylor, D. A. Thermal activation of the visual transduction mechanism in retinal rods. *Nature* **279**, 806-807 (1979).

69 Guha, S. *et al.* Approaches for detecting lysosomal alkalinization and impaired degradation in fresh and cultured RPE cells: evidence for a role in retinal degenerations. *Experimental eye research* **126**, 68-76, doi:10.1016/j.exer.2014.05.013 (2014).

70 Tan, L. X., Toops, K. A. & Lakkaraju, A. Protective responses to sublytic complement in the retinal pigment epithelium. *Proceedings of the National Academy of Sciences of the United States of America* **113**, 8789-8794, doi:10.1073/pnas.1523061113 (2016).

71 Toops, K. A., Tan, L. X., Jiang, Z., Radu, R. A. & Lakkaraju, A. Cholesterol-mediated activation of acid sphingomyelinase disrupts autophagy in the retinal pigment epithelium. *Molecular biology of the cell* **26**, 1-14, doi:10.1091/mbc.E14-05-1028 (2015).

72 Boulanger, A., Liu, S., Henningsgaard, A. A., Yu, S. & Redmond, T. M. The upstream region of the Rpe65 gene confers retinal pigment epithelium-specific expression in vivo and in vitro and contains critical octamer and E-box binding sites. *The Journal of biological chemistry* **275**, 31274-31282, doi:10.1074/jbc.M003441200 (2000).

73 Stec, D. E., Morimoto, S. & Sigmund, C. D. Vectors for high-level expression of cDNAs controlled by tissue-specific promoters in transgenic mice. *BioTechniques* **31**, 256-258, 260 (2001).

74 Parish, C. A., Hashimoto, M., Nakanishi, K., Dillon, J. & Sparrow, J. Isolation and one-step preparation of A2E and iso-A2E, fluorophores from human retinal pigment epithelium. *Proceedings of the National Academy of Sciences of the United States of America* **95**, 14609-14613 (1998).

75 Lois, N., Halfyard, A. S., Bird, A. C., Holder, G. E. & Fitzke, F. W. Fundus autofluorescence in Stargardt macular dystrophy-fundus flavimaculatus. *American journal of ophthalmology* **138**, 55-63, doi:10.1016/j.ajo.2004.02.056 (2004).

76 Zhou, J., Kim, S. R., Westlund, B. S. & Sparrow, J. R. Complement activation by bisretinoid constituents of RPE lipofuscin. *Investigative ophthalmology & visual science* **50**, 1392-1399, doi:iovs.08-2868 [pii]
10.1167/iovs.08-2868 (2009).

77 Klein, R. J. *et al.* Complement Factor H Polymorphism in Age-Related Macular Degeneration. *Science* **308**, 385-389, doi:10.1126/science.1109557 (2005).

78 Edwards, A. O. *et al.* Complement Factor H Polymorphism and Age-Related Macular Degeneration. *Science* **308**, 421-424, doi:10.1126/science.1110189 (2005).

79 Haines, J. L. *et al.* Complement Factor H Variant Increases the Risk of Age-Related Macular Degeneration. *Science* **308**, 419-421, doi:10.1126/science.1110359 (2005).

80 Yates , J. R. W. *et al.* Complement C3 Variant and the Risk of Age-Related Macular Degeneration. *New England Journal of Medicine* **357**, 553-561, doi:doi:10.1056/NEJMoa072618 (2007).

81 Maller, J. B. *et al.* Variation in complement factor 3 is associated with risk of age-related macular degeneration. *Nature genetics* **39**, 1200-1201, doi:10.1038/ng2131 (2007).

82 Hecker, L. A. *et al.* Genetic control of the alternative pathway of complement in humans and age-related macular degeneration. *Human molecular genetics* **19**, 209-215, doi:10.1093/hmg/ddp472 (2009).

83 Gold, B. *et al.* Variation in factor B (BF) and complement component 2 (C2) genes is associated with age-related macular degeneration. *Nature genetics* **38**, 458-462, doi:10.1038/ng1750 (2006).

84 Hageman, G. S. *et al.* A common haplotype in the complement regulatory gene factor H (HF1/CFH) predisposes individuals to age-related macular degeneration. *Proceedings of the National Academy of Sciences of the United States of America* **102**, 7227-7232, doi:10.1073/pnas.0501536102 (2005).

85 Radu, R. A. *et al.* Reductions in serum vitamin A arrest accumulation of toxic retinal fluorophores: a potential therapy for treatment of lipofuscin-based retinal diseases. *Investigative ophthalmology & visual science* **46**, 4393-4401, doi:10.1167/iovs.05-0820 (2005).

86 Flannery, J. G., O'Day, W., Pfeffer, B. A., Horwitz, J. & Bok, D. Uptake, processing and release of retinoids by cultured human retinal pigment epithelium. *Experimental eye research* **51**, 717-728 (1990).

87 Rando, R. R. The biochemistry of the visual cycle. *Chemical reviews* **101**, 1881-1896 (2001).

88 Travis, G. H., Golczak, M., Moise, A. R. & Palczewski, K. Diseases caused by defects in the visual cycle: retinoids as potential therapeutic agents. *Annu Rev Pharmacol Toxicol* **47**, 469-512, doi:10.1146/annurev.pharmtox.47.120505.105225 (2007).

89 Yang, P., Tyrrell, J., Han, I. & Jaffe, G. J. Expression and modulation of RPE cell membrane complement regulatory proteins. *Investigative ophthalmology & visual science* **50**, 3473-3481, doi:10.1167/iovs.08-3202 (2009).

90 Radu, R. A. *et al.* Treatment with isotretinoin inhibits lipofuscin accumulation in a mouse model of recessive Stargardt's macular degeneration. *Proceedings of the National Academy of Sciences of the United States of America* **100**, 4742-4747, doi:10.1073/pnas.0737855100 (2003).

91 Radu, R. A. *et al.* Accelerated accumulation of lipofuscin pigments in the RPE of a mouse model for ABCA4-mediated retinal dystrophies following Vitamin A supplementation. *Investigative ophthalmology & visual science* **49**, 3821-3829 (2008).

92 Foley, S., Li, B., Dehoff, M., Molina, H. & Holers, V. M. Mouse Crry/p65 is a regulator of the alternative pathway of complement activation. *European journal of immunology* **23**, 1381-1384, doi:10.1002/eji.1830230630 (1993).

93 Lock, M. *et al.* Rapid, simple, and versatile manufacturing of recombinant adeno-associated viral vectors at scale. *Human gene therapy* **21**, 1259-1271, doi:10.1089/hum.2010.055 (2010).

94 Radu, R. A. *et al.* Retinal pigment epithelium-retinal G protein receptor-opsin mediates light-dependent translocation of all-trans-retinyl esters for synthesis of visual chromophore in retinal pigment epithelial cells. *The Journal of biological chemistry* **283**, 19730-19738, doi:10.1074/jbc.M801288200 (2008).

95 Hao, W. & Fong, H. K. The endogenous chromophore of retinal G protein-coupled receptor opsin from the pigment epithelium. *The Journal of biological chemistry* **274**, 6085-6090 (1999).

96 Lewis, R. A. *et al.* Genotype/Phenotype analysis of a photoreceptor-specific ATP-binding cassette transporter gene, ABCR, in Stargardt disease. *American journal of human genetics* **64**, 422-434, doi:10.1086/302251 (1999).

97 Fishman, G. A. Fundus flavimaculatus. A clinical classification. *Archives of ophthalmology* **94**, 2061-2067 (1976).

98 Fishman, G. A. in *Electrophysiologic Testing in Disorders of the Retina, Optic nerve and Visual Pathway* (ed G. A. Fishman) 54-56 (The Foundation of the American Academy of Ophthalmology 2001).

99 Lee, B. L. & Heckenlively, J. R. in *Retina-Vitreous-Macula* (eds D. R. Guyer *et al.*) 978-988 (W.B. Saunders, 1999).

100 Burke, T. R. & Tsang, S. H. Allelic and phenotypic heterogeneity in ABCA4 mutations. *Ophthalmic Genet* **32**, 165-174, doi:10.3109/13816810.2011.565397 (2011).

101 Tanna, P., Strauss, R. W., Fujinami, K. & Michaelides, M. Stargardt disease: clinical features, molecular genetics, animal models and therapeutic options. *The British journal of ophthalmology*, doi:10.1136/bjophthalmol-2016-308823 (2016).

102 Fujinami, K. *et al.* Clinical and molecular characteristics of childhood-onset Stargardt disease. *Ophthalmology* **122**, 326-334, doi:10.1016/j.ophtha.2014.08.012 (2015).

103 Strauss, R. W. *et al.* The Natural History of the Progression of Atrophy Secondary to Stargardt Disease (ProgStar) Studies: Design and Baseline Characteristics: ProgStar Report No. 1. *Ophthalmology* **123**, 817-828, doi:10.1016/j.ophtha.2015.12.009 (2016).

104 Allikmets, R. *et al.* Mutation of the Stargardt disease gene (ABCR) in age-related macular degeneration. *Science* **277**, 1805-1807 (1997).

105 Cremers, F. P. *et al.* Autosomal recessive retinitis pigmentosa and cone-rod dystrophy caused by splice site mutations in the Stargardt's disease gene ABCR. *Human molecular genetics* **7**, 355-362 (1998).

106 Allikmets, R. Further evidence for an association of ABCR alleles with age-related macular degeneration. The International ABCR Screening Consortium. *American journal of human genetics* **67**, 487-491 (2000).

107 Klevering, B. J. *et al.* Microarray-based mutation analysis of the ABCA4 (ABCR) gene in autosomal recessive cone-rod dystrophy and retinitis pigmentosa. *Eur J Hum Genet* **12**, 1024-1032, doi:10.1038/sj.ejhg.5201258 (2004).

108 Maugeri, A. *et al.* Mutations in the ABCA4 (ABCR) gene are the major cause of autosomal recessive cone-rod dystrophy. *American journal of human genetics* **67**, 960-966, doi:10.1086/303079 (2000).

109 Martinez-Mir, A. *et al.* Retinitis pigmentosa caused by a homozygous mutation in the Stargardt disease gene ABCR. *Nature genetics* **18**, 11-12, doi:10.1038/ng0198-11 (1998).

110 Charbel Issa, P., Barnard, A. R., Herrmann, P., Washington, I. & MacLaren, R. E. Rescue of the Stargardt phenotype in Abca4 knockout mice through inhibition of vitamin

A dimerization. *Proceedings of the National Academy of Sciences of the United States of America* **112**, 8415-8420, doi:10.1073/pnas.1506960112 (2015).

111 Han, Z., Conley, S. M. & Naash, M. I. Gene therapy for Stargardt disease associated with ABCA4 gene. *Advances in experimental medicine and biology* **801**, 719-724, doi:10.1007/978-1-4614-3209-8_90 (2014).

112 Audo, I. S. *et al.* Early findings in a Phase I/IIa clinical program for Stargardt disease (STGD1, MIM #248200) [abstract]. *Investigative ophthalmology & visual science* **56**, 3819 (2015).

113 Schwartz, S. D. *et al.* Human embryonic stem cell-derived retinal pigment epithelium in patients with age-related macular degeneration and Stargardt's macular dystrophy: follow-up of two open-label phase 1/2 studies. *Lancet* **385**, 509-516, doi:10.1016/s0140-6736(14)61376-3 (2015).

114 Rotenstreich, Y., Fishman, G. A. & Anderson, R. J. Visual acuity loss and clinical observations in a large series of patients with Stargardt disease. *Ophthalmology* **110**, 1151-1158, doi:10.1016/s0161-6420(03)00333-6 (2003).

115 Fujinami, K. *et al.* Clinical and Molecular Analysis of Stargardt Disease With Preserved Foveal Structure and Function. *American journal of ophthalmology* **156**, 487-501.e481, doi:10.1016/j.ajo.2013.05.003 (2013).

116 Westeneng-van Haaften, S. C. *et al.* Clinical and Genetic Characteristics of Late-onset Stargardt's Disease. *Ophthalmology* **119**, 1199-1210, doi:10.1016/j.ophtha.2012.01.005 (2012).

117 Fujinami, K. *et al.* Stargardt Disease with Preserved Central Vision: identification of a putative novel mutation in ATP-binding cassette transporter gene. *Acta ophthalmologica* **89**, e297-e298, doi:10.1111/j.1755-3768.2009.01848.x (2011).

118 Birnbach, C. D., Jarvelainen, M., Possin, D. E. & Milam, A. H. Histopathology and immunocytochemistry of the neurosensory retina in fundus flavimaculatus. *Ophthalmology* **101**, 1211-1219 (1994).

119 Eagle, R. C., Jr., Lucier, A. C., Bernardino, V. B., Jr. & Yanoff, M. Retinal pigment epithelial abnormalities in fundus flavimaculatus: a light and electron microscopic study. *Ophthalmology* **87**, 1189-1200 (1980).

120 McDonnell, P. J., Kivlin, J. D., Maumenee, I. H. & Green, W. R. Fundus flavimaculatus without maculopathy. A clinicopathologic study. *Ophthalmology* **93**, 116-119 (1986).

121 Steinmetz, R. L., Garner, A., Maguire, J. I. & Bird, A. C. Histopathology of incipient fundus flavimaculatus. *Ophthalmology* **98**, 953-956 (1991).

122 Cideciyan, A. V. *et al.* ABCA4-associated retinal degenerations spare structure and function of the human parapapillary retina. *Investigative ophthalmology & visual science* **46**, 4739-4746, doi:10.1167/iovs.05-0805 (2005).

123 Walia, S. & Fishman, G. A. Natural history of phenotypic changes in Stargardt macular dystrophy. *Ophthalmic Genet* **30**, 63-68, doi:10.1080/13816810802695550 (2009).

124 AAO. in *Basic and Clinical Science Course (BCSC)* (ed C.A. McCannel) Ch. Retina, 226-227 (American Academy of Ophthalmology, 2015).

125 Zernant, J. *et al.* Analysis of the ABCA4 genomic locus in Stargardt disease. *Human molecular genetics* **23**, 6797-6806, doi:10.1093/hmg/ddu396 (2014).

126 Fishman, G. A. *et al.* Variation of clinical expression in patients with Stargardt dystrophy and sequence variations in the ABCR gene. *Archives of ophthalmology* **117**, 504-510 (1999).

127 Feng, W., Yasumura, D., Matthes, M. T., LaVail, M. M. & Vollrath, D. Mertk triggers uptake of photoreceptor outer segments during phagocytosis by cultured retinal pigment

epithelial cells. *The Journal of biological chemistry* **277**, 17016-17022, doi:10.1074/jbc.M107876200 (2002).

128 Connell, G. *et al.* Photoreceptor peripherin is the normal product of the gene responsible for retinal degeneration in the rds mouse. *Proceedings of the National Academy of Sciences of the United States of America* **88**, 723-726 (1991).

129 Travis, G. H., Sutcliffe, J. G. & Bok, D. The retinal degeneration slow (rds) gene product is a photoreceptor disc membrane-associated glycoprotein. *Neuron* **6**, 61-70 (1991).

130 Saari, J. C., Bredberg, L. & Garwin, G. G. Identification of the endogenous retinoids associated with three cellular retinoid-binding proteins from bovine retina and retinal pigment epithelium. *The Journal of biological chemistry* **257**, 13329-13333 (1982).

131 Jin, M., Li, S., Moghrabi, W. N., Sun, H. & Travis, G. H. Rpe65 is the retinoid isomerase in bovine retinal pigment epithelium. *Cell* **122**, 449-459, doi:10.1016/j.cell.2005.06.042 (2005).

132 Belyaeva, O. V., Johnson, M. P. & Kedishvili, N. Y. Kinetic analysis of human enzyme RDH10 defines the characteristics of a physiologically relevant retinol dehydrogenase. *The Journal of biological chemistry* **283**, 20299-20308, doi:10.1074/jbc.M800019200 (2008).

133 Farjo, K. M., Moiseyev, G., Takahashi, Y., Crouch, R. K. & Ma, J. X. The 11-cis-retinol dehydrogenase activity of RDH10 and its interaction with visual cycle proteins. *Investigative ophthalmology & visual science* **50**, 5089-5097, doi:10.1167/iovs.09-3797 (2009).

134 Palczewska, G. *et al.* Receptor tyrosine kinase MERTK is not required for transfer of bis-retinoids to the retinal pigmented epithelium. *Journal of Biological Chemistry*, doi:10.1074/jbc.M116.764563 (2016).

135 McBee, J. K. *et al.* Isomerization of all-trans-retinol to cis-retinols in bovine retinal pigment epithelial cells: dependence on the specificity of retinoid-binding proteins. *Biochemistry* **39**, 11370-11380 (2000).

136 Kaylor, J. J. *et al.* Blue light regenerates functional visual pigments in mammals through a retinyl-phospholipid intermediate. *Nature communications* **8**, 16, doi:10.1038/s41467-017-00018-4 (2017).

137 Calame, M. *et al.* Retinal degeneration progression changes lentiviral vector cell targeting in the retina. *PloS one* **6**, e23782, doi:10.1371/journal.pone.0023782 (2011).

138 Balaggan, K. S. *et al.* Stable and efficient intraocular gene transfer using pseudotyped EIAV lentiviral vectors. *The journal of gene medicine* **8**, 275-285, doi:10.1002/jgm.845 (2006).

139 Carr, A. J. *et al.* Protective effects of human iPS-derived retinal pigment epithelium cell transplantation in the retinal dystrophic rat. *PloS one* **4**, e8152, doi:10.1371/journal.pone.0008152 (2009).

140 Radu, R. A., Hu, J., Jiang, Z. & Bok, D. Bisretinoid-mediated complement activation on retinal pigment epithelial cells is dependent on complement factor H haplotype. *The Journal of biological chemistry* **289**, 9113-9120, doi:10.1074/jbc.M114.548669 (2014).

141 Mandal, M. N. & Ayyagari, R. Complement factor H: spatial and temporal expression and localization in the eye. *Investigative ophthalmology & visual science* **47**, 4091-4097, doi:10.1167/iovs.05-1655 (2006).

142 Vogt, S. D. *et al.* Retinal pigment epithelial expression of complement regulator CD46 is altered early in the course of geographic atrophy. *Experimental eye research* **93**, 413-423, doi:10.1016/j.exer.2011.06.002 (2011).

143 Morgan, B. P. The membrane attack complex as an inflammatory trigger. *Immunobiology* **221**, 747-751, doi:10.1016/j.imbio.2015.04.006 (2016).

144 Lueck, K. *et al.* Sub-lytic C5b-9 induces functional changes in retinal pigment epithelial cells consistent with age-related macular degeneration. *Eye* **25**, 1074-1082, doi:10.1038/eye.2011.109 (2011).

145 Kunchithapautham, K. & Rohrer, B. Sublytic membrane-attack-complex (MAC) activation alters regulated rather than constitutive vascular endothelial growth factor (VEGF) secretion in retinal pigment epithelium monolayers. *The Journal of biological chemistry* **286**, 23717-23724, doi:10.1074/jbc.M110.214593 (2011).

146 Vogt, S. D., Barnum, S. R., Curcio, C. A. & Read, R. W. Distribution of complement anaphylatoxin receptors and membrane-bound regulators in normal human retina. *Experimental eye research* **83**, 834-840, doi:10.1016/j.exer.2006.04.002 (2006).

147 Georgiannakis, A. *et al.* Retinal Pigment Epithelial Cells Mitigate the Effects of Complement Attack by Endocytosis of C5b-9. *Journal of immunology* **195**, 3382-3389, doi:10.4049/jimmunol.1500937 (2015).

148 Sparrow, J. R. *et al.* Quantitative fundus autofluorescence in mice: correlation with HPLC quantitation of RPE lipofuscin and measurement of retina outer nuclear layer thickness. *Investigative ophthalmology & visual science* **54**, 2812-2820, doi:10.1167/iovs.12-11490 (2013).

149 Bavik, C. *et al.* Visual Cycle Modulation as an Approach toward Preservation of Retinal Integrity. *PloS one* **10**, e0124940, doi:10.1371/journal.pone.0124940 (2015).

150 Fritsche, L. G. *et al.* A subgroup of age-related macular degeneration is associated with mono-allelic sequence variants in the ABCA4 gene. *Investigative ophthalmology & visual science* **53**, 2112-2118, doi:10.1167/iovs.11-8785 (2012).

151 Gehrs, K. M., Anderson, D. H., Johnson, L. V. & Hageman, G. S. Age-related macular degeneration--emerging pathogenetic and therapeutic concepts. *Ann Med* **38**, 450-471, doi:P30P0084J262W715 [pii]

10.1080/07853890600946724 (2006).

152 Fritsche, L. G. *et al.* An imbalance of human complement regulatory proteins CFHR1, CFHR3 and factor H influences risk for age-related macular degeneration (AMD). *Human molecular genetics* **19**, 4694-4704, doi:10.1093/hmg/ddq399 (2010).